© 2019. Published by The Company of Biologists Ltd | Journal of Cell Science (2020) 133, jcs236141. doi:10.1242/jcs.236141

RESEARCH ARTICLE

SPECIAL ISSUE: CELL BIOLOGY OF THE IMMUNE SYSTEM

Discovery of aspirin-triggered eicosanoid-like mediators in a *Drosophila* metainflammation blood tumor model

Silvio Panettieri[1,2,§], Indira Paddibhatla[3,4,*,§], Jennifer Chou[4], Roma Rajwani[4], Rebecca S. Moore[4,‡], Tamara Goncharuk[4], George John[1,2,¶] and Shubha Govind[4,5,¶]

ABSTRACT

Epidemiologic studies have linked the use of aspirin to a decline in chronic inflammation that underlies many human diseases, including some cancers. Aspirin reduces the levels of cyclooxygenase-mediated pro-inflammatory prostaglandins, promotes the production of pro-resolution molecules, and triggers the production of anti-inflammatory electrophilic mono-oxygenated (EFOX) lipid mediators. We investigated the effects of aspirin in fruit fly models of chronic inflammation. Ectopic Toll/NF-κB and JAK/STAT signaling in mutant *D. melanogaster* results in overproliferation of hematopoietic blood progenitors resulting in the formation of granuloma-like tumors. Ectopic JAK-STAT signaling also leads to metabolic inflammation. We report that aspirin-treated mutant flies experience reduction in metabolic inflammation, mitosis, ectopic immune signaling, and macrophage infiltration. Moreover, these flies synthesize 13-HODE, and aspirin triggers 13-oxoODE (13-EFOX-L_2) production. Providing the precursor of 13-HODE, linoleic acid, or performing targeted knockdown of the transcription factor STAT in inflammatory blood cells, boosts 13-EFOX-L_2 levels while decreasing metabolic inflammation. Thus, hematopoietic cells regulate metabolic inflammation in flies, and their effects can be reversed by pharmaceutical or dietary intervention, suggesting deep phylogenetic conservation in the ability of animals to resolve inflammation and repair tissue damage. These findings can help identify novel treatment targets in humans.

KEY WORDS: Eicosanoid, EFOX, 13-HODE, 13-oxoODE, NF-κB, Fatty acid, Aspirin, Systemic inflammation, Resolution, Macrophages, *Drosophila*

INTRODUCTION

As part of the innate immune system of animals, acute inflammation targets parasites and microbes and repairs injured tissues. Circulating macrophages and neutrophils migrate to sites of infection or injury where they initiate acute inflammation either to phagocytose and clear invading organisms, or to sequester parasite or cellular debris. Mammals and *Drosophila melanogaster* rely on the archetypal pro-inflammatory NF-κB signaling pathway to activate the inflammation response (Lawrence, 2009). Canonical NF-κB signaling employs Toll and Toll-like receptors (TLRs), which, when bound by pathogen-derived ligand in mammals, mediate the release (from their I-κB inhibitors) and nuclear import of nuclear factor (NF)-κB. NF-κB activates pro-inflammatory pattern of gene expression (Baker et al., 2011; Lawrence, 2009). Pathogen receptors in flies also activate the Toll-NF-κB signaling pathway for host defense (Cherry and Silverman, 2006; Govind, 2008; Govind and Nehm, 2004; Lemaitre and Hoffmann, 2007).

A key target of pro-inflammatory NF-κB activation in mammals is the cyclooxygenase-2 (*COX-2*; also known as prostaglandin-endoperoxide synthase 2, *PTGS2*) promoter. COX-2 catalyzes the rate-limiting step in the conversion of the polyunsaturated C20:4 ω-6 fatty acid (FA) arachidonic acid (AA) to pro- and anti-inflammatory prostanoids (Groeger et al., 2010). AA, an important component of the phospholipids in the plasma membrane, is derived from the dietary omega (ω)-6 FA linoleic acid (LA). NF-κB-mediated induction of *COX-2* integrates eicosanoid-mediated signaling with NF-κB signaling. Toll and NF-κB signaling also responds to free fatty acid levels in the blood. For example, saturated (but not unsaturated) fatty acids activate TLR4 and its downstream mediators, and NF-κB p65 (also known as RELA) activation triggers *COX-2* expression (Lee et al., 2001, 2003). Since Toll receptors sense both pathogens and nutrients in mammals, diet and energy balance are closely integrated with innate immunity and inflammation (Baker et al., 2011; Hotamisligil, 2006; Shapiro et al., 2011). Aspirin (acetylsalicylic acid, ASA) inhibits the pro-inflammatory effects of prostanoids by acetylating COX-1 and -2 activities (Alfonso et al., 2014).

The second biochemical effect of aspirin is to promote the resolution of acute inflammation. A new class of specialized pro-resolving mediators (SPMs) are formed in the presence of acetylated COX-2. Derived from C20 or C22 ω-3 and ω-6 FAs, SPMs include lipoxins, resolvins, protectins and maresins. SPMs boost efferocytosis, promote phagocytosis of microbes, and limit neutrophil-mediated tissue damage; reviewed in Serhan et al. (2015). In human cells, acetylated COX-2 also triggers the production of a family of electrophilic mono-oxygenated (EFOX) lipid mediators, including 17- and 13-EFOX, derived from ω-3 C22:6 docasahexanoic acid (DHA) (Delmastro-Greenwood et al., 2014). These dual anti-inflammatory and pro-resolution roles of aspirin explain how dietary ω-3 FAs or aspirin stalls inflammation and supports well-being in humans (Delmastro-Greenwood et al., 2014; Groeger et al., 2010). They also expose the diversity of eicosanoid and eicosanoid-like lipid mediators and the complexity of their cell-specific effects in maintaining normal organism-level physiology. How are the pro- and anti-inflammatory effects of

[1]Department of Chemistry & Biochemistry, The City College of New York, New York, NY 10031, USA. [2]PhD Program in Chemistry, The Graduate Center, City University of New York, 365 Fifth Avenue, New York, NY 10016, USA. [3]PhD Program in Biology, Graduate Center, City University of New York, 365 Fifth Avenue, New York, NY 10016, USA. [4]Biology Department, The City College of New York, 160 Convent Avenue, New York, NY 10031, USA. [5]PhD Programs in Biology & Biochemistry, The Graduate Center, City University of New York, 365 Fifth Avenue, New York, NY 10016, USA.
*Present address: Department of Biochemistry, School of Life Sciences, University of Hyderabad, Gachibowli, Hyderabad 500046, India. ‡Present address: Department of Molecular Biology, Princeton University, Princeton, NJ 08544, USA. §These authors contributed equally to this work

¶Authors for correspondence (sgovind@ccny.cuny.edu; gjohn@ccny.cuny.edu)

S.P., 0000-0001-6736-0455; I.P., 0000-0002-3057-2160; J.C., 0000-0003-3351-5855; R.R., 0000-0002-3729-8213; R.S.M., 0000-0003-3155-3436; T.G., 0000-0002-5747-7227; G.J., 0000-0002-0382-1256; S.G., 0000-0002-6436-639X

Received 11 July 2019; Accepted 20 September 2019

Journal of Cell Science (2020) 133, jcs236141. doi:10.1242/jcs.236141

eicosanoid family members precisely integrated with the metabolic and immune pathways *in vivo*? How are their effects unified from cellular to tissue and organism levels (e.g. from inflammatory macrophages to adipose tissue)? Because of their inherent diversity and cellular complexity, vertebrate models do not lend themselves to straightforward resolution of such questions.

To systematically address these issues, we used *D. melanogaster* models with proven hallmarks of chronic inflammation (CI). In one such CI mutant (*Ubc9*, which encodes the E2 SUMO-conjugating enzyme), Toll-NF-κB dependent regulatory mechanisms underlying acute inflammation is dysregulated. CI in *Ubc9* is characterized by (1) high levels of the pro-mitotic and pro-inflammatory cytokine and Toll ligand Spätzle (Spz) and the Spätzle Processing Enzyme (SPE); (2) constitutive expression of the Toll-NF-κB target gene *Drosomycin* (*Drs*) in the liver-like larval fat body; (3) niche-independent hematopoietic overgrowth of the lymph gland progenitors; and (4) loss of basement membrane integrity of the fat body and blood cell infiltration into the diseased tissue (Kalamarz et al., 2012; Paddibhatla et al., 2010). Similar defects have been described in *hopscotch*$^{Tum\text{-}l}$ mutants with hyperactive JAK-STAT signaling (Chiu et al., 2005; Harrison et al., 1995; Luo et al., 1995).

Flies also react to metabolic stress in ways similar to humans. In response to a high-sugar diet (but not to excess dietary fat or protein), *Drosophila* develop signs of metabolic inflammation (or metainflammation) where cellular and molecular phenotypes resemble the pathophysiology of type-2 diabetes mellitus (Baker et al., 2011; Musselman et al., 2011). High-sugar-fed larvae exhibit an altered metabolism and the cells of their fat body organ display larger-sized lipid droplets (LDs, which store and mobilize fat in animal cells; Musselman et al., 2011). Therefore, mechanistically, sugar-induced metabolic dysregulation in flies resembles insulin resistance in humans (Kim and Choe, 2014; Musselman et al., 2011; Shapiro et al., 2011).

Given that flies exhibit hallmarks of parasite-induced inflammatory and diet-induced metainflammatory responses, we hypothesized that these phenotypes are sensitive to aspirin, and aspirin might activate and coordinate the intrinsic healing mechanisms of the flies as it does in mammals. While flies lack FAs longer than C18 (AA, DHA, etc.) (Shen et al., 2010) and eicosanoids have not been reported from *Drosophila*, prostaglandin administration rescues the loss-of-function phenotype of a human *COX-1*-like fly gene *peroxinectin* (*pxt*) (Tootle and Spradling, 2008), suggesting that flies possess primordial eicosanoid-based mechanisms through which aspirin might act. In addition, C20 polyunsaturated fatty acid (PUFA)-fed flies generate hydroxyeicosatetraenoic acid (13-HETE) (Tan et al., 2016), an AA metabolite, suggesting that flies express enzymes for eicosanoid synthesis. Our computational studies show that many functional enzymes for eicosanoid biosynthesis are encoded in the fly genome, including two other COX-like enzymes in addition to Pxt (Scarpati et al., 2019). We therefore analyzed inflammation readouts in flies after aspirin treatment and searched for anti-inflammatory C18-derived PUFAs.

Here, we show that aspirin has dose-dependent and molecular-, cell-, and organ-specific effects with striking parallels to its effects in mammals. We also show, for the first time, that flies produce the LA-derived PUFA, 13-HODE, and aspirin increases 13-HODE levels, while also triggering the production of its oxidized analog 13-oxoODE (herein called 13-EFOX-L_2). The efficacy of aspirin in resolving inflammation and repairing tissue damage in fruit flies suggests genetic and biochemical conservation underlying these processes across the animal kingdom. Furthermore, like flies, mammals may produce LA-derived electrophilic FAs, with beneficial anti-inflammatory roles in organs with high LA levels. Unbiased genetic screens in *Drosophila* that report the links between inflammation, diet and drug action, therefore, might have translational significance in identifying new therapies for inflammation-based human diseases.

RESULTS

Wild-type *Canton S* flies tolerate a wide range of orally administered aspirin. We found that at 5 mM aspirin, 65% of the animals eclosed to adulthood while 42% of pupae became adults at 55 mM. In the experiments described below, 0.5 nM to 1 mM aspirin was added to fly food (see Materials and Methods for additional details). Aspirin uptake was confirmed by covalently conjugating it to Rhodamine B. Dissected hematopoietic and fat body cells did not retain the unconjugated dye *ex vivo*, but Rhodamine B–aspirin (Rh-ASA) localized to the perinuclear regions in both cell types (Fig. S1).

Aspirin inhibits hematopoietic overgrowth and restores regulation of Toll-NF-κB signaling in *Ubc9* mutants

We introduced 0.5 nM or 5.5 µM aspirin to the diet of developmentally synchronized cultures of heterozygote and inflammatory tumor-producing homozygous *Ubc9* mutant larvae, and examined its effects on tumor abundance (penetrance) and sizes (tumor projection area or expressivity), and gene expression. Aspirin (0.5 nM and 5.5 µM) treatment resulted in a remarkable increase in tumor-free animals (0–2 tumors/animal compared to three or more tumors in untreated animals; Fig. 1A,B,D). At both aspirin concentrations, tumor projection area shrank by more than 60% (Fig. 1C,E). Tumor penetrance remained unaffected with salicylic acid (SA) treatment (see Materials and Methods).

We have previously shown that *Ubc9* tumors are derived from overproliferating lymph gland lobes (Kalamarz et al., 2012). Reduction in tumor penetrance by aspirin treatment (Fig. 1A–E) was also reflected in the shrinkage of lymph gland lobes and in the restoration of lymph gland morphology (Fig. 1F). Relative to heterozygous lymph glands, *76B>GFP*-marked mutant *Ubc9* lymph glands have an expanded GFP-positive progenitor population with many inflammatory lamellocytes (Fig. 1F) (Kalamarz et al., 2012). Treatment with 0.5 nM aspirin reduced the progenitor and mature blood cell populations (Fig. 1F). The size of the lymph gland lobes was reduced; while the projection areas of anterior lobes did not differ significantly (P=0.34), the first set of posterior lobes shrank in size [P=0.005; 20,907.04±1838.24 µm^2 in untreated versus 9221.45±3238.40 µm^2 in 0.5 nM aspirin treated animals (mean±s.d.); three biological replicates, four to six lobes per replicate]. Thus, administration of aspirin restricted lymph gland overgrowth and tumor development.

Constitutive signaling in *Ubc9* fat bodies results in the activation of *Drs-GFP* as well as infiltration of macrophages and lamellocytes on the diseased fat body (Chiu et al., 2005; Paddibhatla et al., 2010). Both these phenotypes are rescued by aspirin. At day 6, there was a ∼40% decrease in the percentage of *Drs-GFP*-positive larvae (0.5 nM ASA; Fig. 1G,H). This decrease in *Drs-GFP* expression correlated with reduced infiltration of blood cells into the fat body adipocytes (Fig. 1I). Thus, it appears that like in mammalian cells (Kopp and Ghosh, 1994), aspirin inhibits chronic inflammation in flies by modulating the Toll-NF-κB axis.

Aspirin counteracts constitutive immune signaling in *hopscotch*$^{Tum\text{-}l}$ blood cells; it is anti-mitotic, and improves organismal viability

To corroborate the effects of aspirin in another genetic background and understand how it promotes healing and tissue repair, we turned

Journal of Cell Science (2020) 133, jcs236141. doi:10.1242/jcs.236141

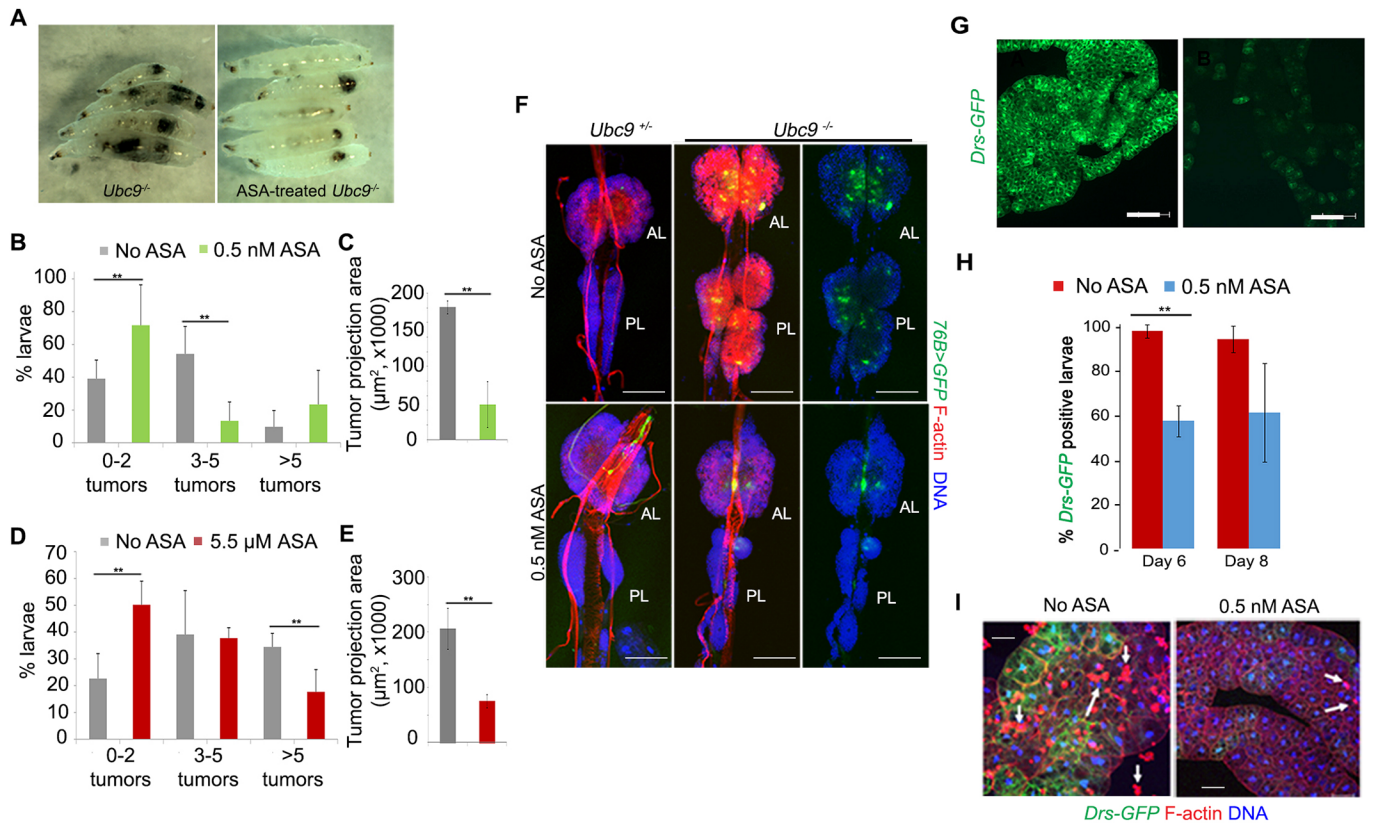

Fig. 1. Anti-inflammatory effects of aspirin in the *Ubc9* model of chronic inflammation. (A) Untreated (left) and 0.5 nM aspirin (ASA)-treated 8-day-old *Ubc9* larvae showing clearance of some, but not all tumors. (B–E) Tumor penetrance (B,D) and tumor size (average of measured projection areas of all tumors) (C,E) in 8-day old *Ubc9* larvae. For tumor penetrance (B,D), the proportion of mutants with 0–2 tumors to 5 or more tumors is shown. Data are from three biological replicates. The number of animals for each replicate and treatment ranged from 5–20. Tumor penetrance and tumor size data were obtained from the same animals. For C, the mean±s.d. projection area values for the 8-day-old *Ubc9* tumors from the 0.5 nM aspirin dataset were 181,024±8571 μm^2 and 48,144±31,459 μm^2 for untreated and treated samples, respectively. The corresponding values from the 5.5 μM aspirin dataset for 8-day *Ubc9* animals (E) were 206,308±37,011 μm^2 and 75,251±11,943 μm^2 for untreated and treated samples, respectively. ***P*<0.05. The color of the bar refers to treatment regimes as shown. (F) Aspirin shrinks the expanded hematopoietic population in *Ubc9* mutants. Anterior and posterior lymph gland lobes from untreated or 0.5 nM aspirin-treated control or mutant animals are shown. The progenitor population here is marked with *76B>GFP*. Cells are stained with phalloidin to visualize actin-rich lamellocytes and the dorsal vessel; Hoechst 33258 stain identifies nuclei. AL, anterior lobes; PL, posterior lobes. Right panels do not show the red signal in mutant glands. Scale bars: 100 μm. (G,H) Aspirin administration attenuates *Drs-GFP* reporter expression in the *Ubc9* fat body. (G) Fat body tissue from a 6-day-old *Ubc9* larva after 0.5 nM aspirin administration shows a significant reduction in the *Drs-GFP* expression (right) compared to fat body tissue from an untreated (left) *Ubc9* larva. Scale bars: 100 μm. (H) Percentage of larvae with *Drs-GFP* expression. The entire fat body was dissected to study GFP expression. A fat body was considered GFP-positive if at least ten cells expressed GFP in the entire organ. The bars represent mean±s.e.m. from three biological replicates. At day 6, 96.7±3% (untreated) and 56.9±16% (0.5 nM aspirin-treated) larvae were GFP positive. At the 8-day time point, 93.3±7% (untreated) and 60.7±23% (0.5 nM aspirin-treated) larvae were GFP positive. The number of 6-day-old larvae per replicate ranged from 8 to 19; the number of 8-day-old larvae used per replicate ranged from 5 to 18 (few 8-day-old animals survive). *P*=0.03 for 6-day-old larvae; *P*=0.12 in 8-day-old larvae (Student's *t*-test). (I) *Drs-GFP* fat bodies from untreated (left) and aspirin-treated (right) 8-day-old *Ubc9* larvae show simultaneous reduction in blood cell infiltration (Rhodamine–phalloidin; arrows) and *GFP* expression. Scale bars: 150 μm.

to the *hopscotch*$^{Tum\text{-}l}$ (*hop*$^{Tum\text{-}l}$ or simply *Tum-l*) mutant, where JAK-STAT signaling is hyperactive due to a dominant gain-of-function point mutation (Luo et al., 1995). In these mutants, hyperactive STAT activity expands the hematopoietic progenitor population (Anderson et al., 2017; Harrison et al., 1995; Luo et al., 1995) and lymph gland dysplasia leads to tumor development and partial lethality (Irving et al., 2005; Luo et al., 1995) (Fig. 2A–C). Microarray analysis revealed high expression of key Toll pathway genes (*SPE*, *spz*, *Toll* and *Dif*) in *hop*$^{Tum\text{-}l}$ mutants (Fig. 2D) (Irving et al., 2005).

To determine whether the expanded hematopoietic population is fundamental to chronic inflammation in *hop*$^{Tum\text{-}l}$ mutants and whether systemic effects compromise viability, we depleted *STAT* and *Toll* pathway gene expression (*SPE*, *spz*, *Toll* and *dl*) in this expanding hematopoietic population by means of RNAi knockdown (KD; *hop*$^{Tum\text{-}l}$ *msn>mCD8-GFP*, *RNAi*; Fig. 2A). We compared the viability of KD animals with outcrossed *hop*$^{Tum\text{-}l}$ mutants without KD. Viability of progeny from the *y w* outcross was no different if *white*, *ebony* or *GFP* RNAi was expressed (Fig. S2A). In contrast, compared to the control *y w* outcross, *hop*$^{Tum\text{-}l}$ mutants were more viable when pro-inflammatory STAT or NF-κB signaling was knocked down. The most significant gains were seen with *STAT*, *SPE* and *spz* knockdown in blood cells (Fig. 2E). These results suggest a potential downstream or cooperative role of the Spz-Toll-Dorsal/Dif axis with STAT in *hop*$^{Tum\text{-}l}$ blood cells. Aspirin treatment (1 μM) of *hop*$^{Tum\text{-}l}$ animals reduced the mitotic index in circulating blood cells (Fig. 2F). These results confirm that, as such, the effects of aspirin are not limited to a specific genetic background, but instead its biological effects must be meditated by molecular pathways common to both mutants.

Immune responses in mammals can modulate insulin signaling and nutrient storage (Cressler et al., 2014), and conversely, immune

Journal of Cell Science (2020) 133, jcs236141. doi:10.1242/jcs.236141

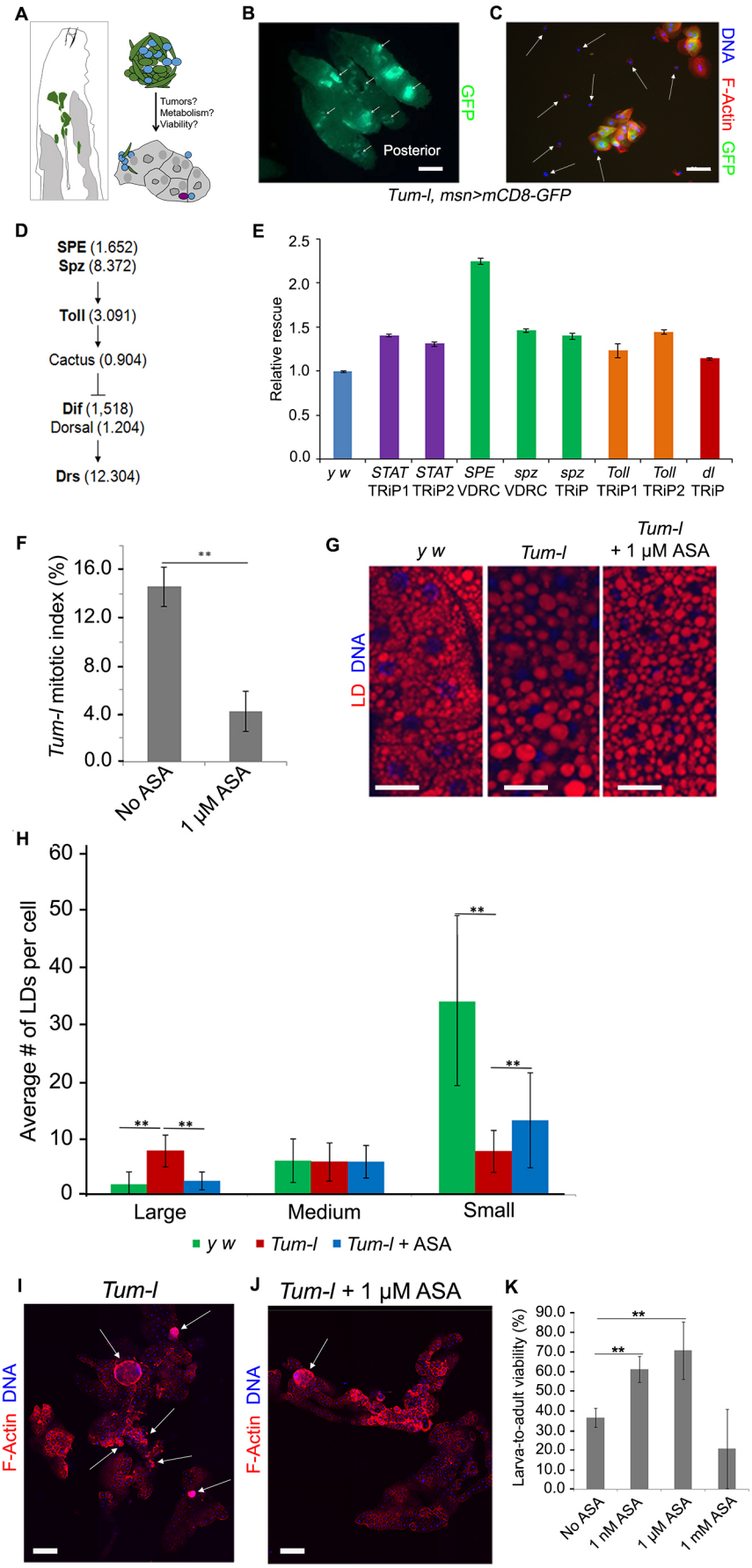

Fig. 2. Aspirin is anti-inflammatory in *hop*$^{Tum\text{-}l}$ larvae and improves viability. (A) Schematic showing immune organs present in a *hop*$^{Tum\text{-}l}$ *msn>mCD8-GFP* larva. The expanded hematopoietic cells are found in the hemolymph and around the fat body. An *msn-GAL4* transgene allows targeted manipulation of gene expression in progenitors of inflammatory lamellocytes. The effects of such manipulation on tumorigenesis, viability and metainflammation can thus be examined. (B) GFP-positive hematopoietic tumors (arrows) in 6-day-old *hop*$^{Tum\text{-}l}$ *msn>mCD8-GFP* whole larvae. Scale bar: 1 mm. (C) An aggregate of mutant blood cells from a drop of hemolymph gently bled from a 6-day-old third-instar larva showing GFP-positive lamellocytes and GFP-negative macrophages (white arrows). Only these two cell types are present in this preparation. Scale bar: 50 µm. (D) Microarray data summarized from reference (Irving et al., 2005) performed on *hop*$^{Tum\text{-}l}$ revealing that Toll pathway components are transcriptionally active. A significant increase (>1.5-fold) was observed for *SPE*, *spz*, *Toll* and *Dif* genes. (E) Relative viability of adult *hop*$^{Tum\text{-}l}$ *msn>mCD8-GFP* males at 27°C with RNAi compared to viability of control *hop*$^{Tum\text{-}l}$ males from an outcross of *hop*$^{Tum\text{-}l}$/*FM7* females and *y w* males without RNAi. Bars represent mean±s.e.m.; $P<0.05$ (Student's *t*-test) for all pairwise comparisons across three biological replicates. The number of males scored for a given replicate ranged from 76 to 279. (F) Mitotic index in blood cell smears of *hop*$^{Tum\text{-}l}$ *msn>mCD8-GFP* animals after 1 µM aspirin (ASA) treatment (mean±s.d.; three biological replicates, 20 larvae per replicate, and more than 800 macrophages per treatment). $^{**}P<0.01$ (Student's *t*-test). (G) Representative images of Nile Red-stained larval fat body adipocytes from untreated *y w*, and untreated and 1 µM aspirin-treated *hop*$^{Tum\text{-}l}$ *msn>mCD8-GFP* animals. Scale bars: 30 µm. (H) Average number of large, medium or small LDs per cell from fat bodies of untreated *y w* animals, and untreated and 1 µM aspirin-treated *hop*$^{Tum\text{-}l}$ *msn>mCD8-GFP* animals. At least 30 fat body cells per animal were scored and mean±s.d. was computed using six animals. Three biological replicates were performed. $^{**}P<0.001$ (Student's *t*-test.). (I,J) Confocal images of Rhodamine–phalloidin and Hoechst 33258-stained fat body from untreated (I) or 1 µM aspirin-treated (J) *hop*$^{Tum\text{-}l}$ *msn>mCD8-GFP* animals. Fewer aggregates and tumors (arrows) were present on the organ from treated animals and the organ morphology is closer to normal. (K) Larval-to-adult viability of *hop*$^{Tum\text{-}l}$ *msn>mCD8-GFP* animals upon systemic aspirin treatment (mean±s.d. is shown across four biological replicates; $n>38$ larvae per replicate). $^{**}P<0.05$ (Student's *t*-test).

Journal of Cell Science (2020) 133, jcs236141. doi:10.1242/jcs.236141

pathways are activated in response to nutrient stress (Gregor and Hotamisligil, 2011). We wondered whether LD sizes are affected in $hop^{Tum\text{-}l}$ mutants and if aspirin might reverse these effects. In flies, the diabetes-like metabolic state is reflected in larger LDs in larval fat bodies of animals consuming high dietary glucose (Musselman et al., 2011). Adipocytes of the $hop^{Tum\text{-}l}$ fat body form many large and distorted LDs without added dietary glucose (Fig. 2G,H). Additionally, the mutant fat body loses integrity and intercellular adhesion; several portions of the organ detach from the main organ (Fig. 2I). However, administration of 1 µM aspirin restored a significant portion of the small LD population and there were fewer large LDs (Fig. 2G,H); aspirin also restored the overall morphology of the organ (Fig. 2I,J). These results suggest that as in vertebrate models and in human trials, where anti-inflammatory therapies restore metabolic function (Bozza et al., 1996; Gregor and Hotamisligil, 2011), aspirin treatment in flies also reduces metabolic stress.

Encouraged by the strong and consistent anti-tumor and anti-inflammatory effects of aspirin at the molecular, cellular and organ levels in two inflammation models, we asked whether these effects might translate to benefits at the organism level and whether aspirin improves the viability of $hop^{Tum\text{-}l}$ animals. 1 nM and 1 µM aspirin improved the viability of $hop^{Tum\text{-}l}$ animals to adulthood (i.e. the proportion of flies that eclosed compared to the no treatment controls) (Fig. 2K) and these gains paralleled viability increments in the targeted knockdown experiments (Fig. 2E). This correlation suggests that the salutary effects of aspirin are, in part, realized by blocking the systemic pro-inflammatory effects of blood cells. We hypothesized that, in addition to reducing mitosis and shrinking the pro-inflammatory blood cell population, aspirin might trigger oxylipid production whose anti-inflammatory effects may be realized in other parts of the body and possibly the entire organism. We tested this idea in biochemical experiments.

Discovery of 13-HODE and 13-EFOX-L_2 in fly larvae

Because *D. melanogaster* lack FAs longer than C18 (Shen et al., 2010), we searched for non-classical anti-inflammatory lipid mediators derived from unsaturated C18 precursors linoleic acid (LA) and α-linolenic acid (ALA), present in the normal fly diet (Shen et al., 2010). Oxidized derivatives of LA and ALA [13-hydroxyoctadecadienoic acid (13-HODE) and 13-hydroxyoctadecatrienoic acid (13-HOTrE), respectively; see structures in Fig. 3A and Fig. S3A] are bioactive and exert potent anti-inflammatory effects in mammals (Bozza et al., 1996; Delmastro-Greenwood et al., 2014; Dennis and Norris, 2015; Groeger et al., 2010; Serhan et al., 2015). In liquid chromatogragphy tandem mass spectrometry (LC-MS/MS)-based targeted lipidomics of larval extracts, we did not detect 13-HOTrE in wild-type or mutant larvae, but discovered that untreated third-instar wild-type, control, and $hop^{Tum\text{-}l}$ larvae produce 13-HODE at levels comparable to mammalian cells (~40 nM; Fig. 3B; Figs S2D and S3B,D; Yuan et al., 2010).

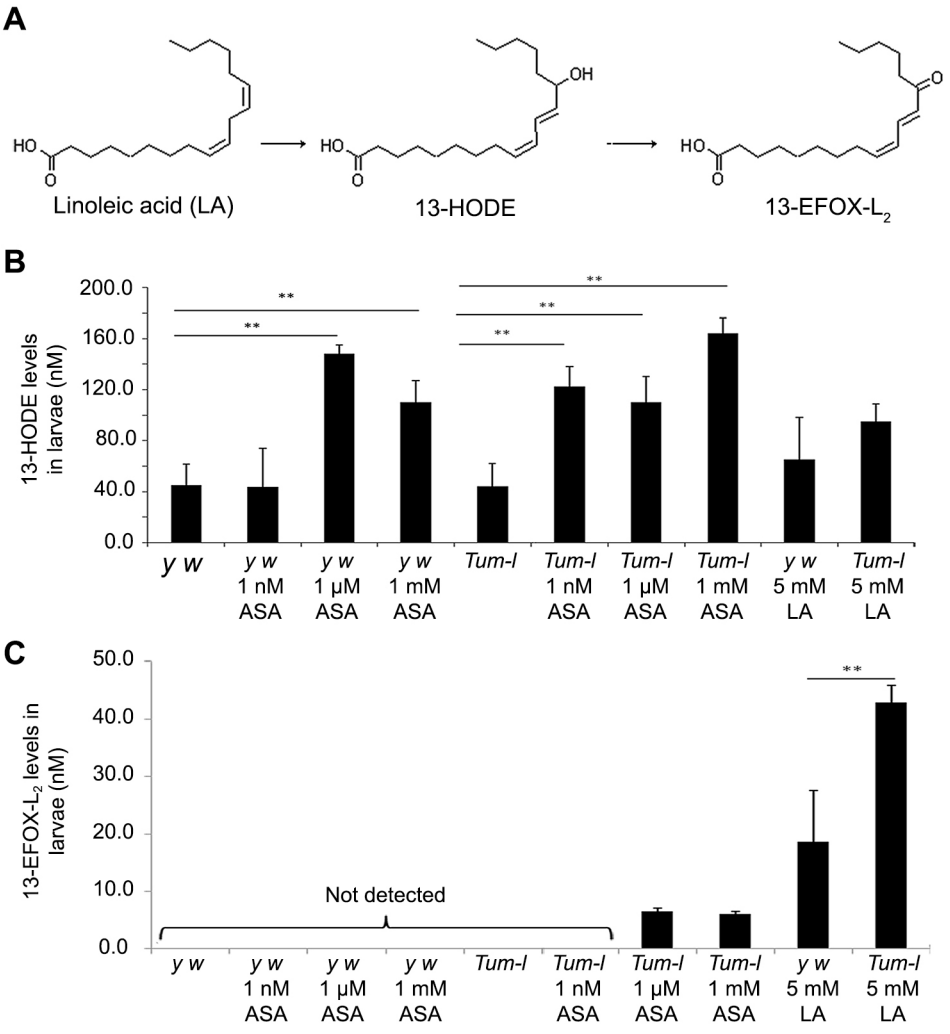

Fig. 3. Aspirin-triggered production of 13-HODE and 13-EFOX-L_2. (A) LA is first converted into 13-HODE by COX-2 action, and then further oxidized to 13-EFOX-L_2. This proposed scheme is based on Groeger et al. (2010). (B,C) Quantification of 13-HODE (B) and 13-EFOX-L_2 (C) levels in *y w* and $hop^{Tum\text{-}l}$ animals without or with 1 nM, 1 µM or 1 mM aspirin (ASA) treatment (n>200 larvae per measurement per compound, mean±s.d. across three to five biological replicates, $^{**}P$<0.05; one-way ANOVA was applied).

Journal of Cell Science (2020) 133, jcs236141. doi:10.1242/jcs.236141

Application of an enantiomer-specific antibody in ELISA experiments (Enzo Life Sciences) confirmed the presence of 13(S)-HODE in both isolated larval fat bodies and the remaining organs of untreated larvae, suggesting its wide occurrence in the body. Chiral LC-MS/MS analysis resolved the R and S enantiomers of 13-HODE, and showed that 13(S)-HODE was twice as abundant as 13(R)-HODE regardless of genetic background or aspirin treatment (Fig. S3D, and data not shown). This enantiomeric imbalance indicates that at least some of the oxidation product may be generated enzymatically. In mammalian models, the R and S enantiomers demonstrate pro- or anti-inflammatory activities.

Quantitative LC-MS/MS further revealed that 13-HODE levels increase 3-fold in control and $hop^{Tum\text{-}l}$ larvae upon treatment with 1 µM and 1 mM aspirin (Fig. 3B). At 1 nM aspirin, however, a comparable 3-fold increase is observed only in the $hop^{Tum\text{-}l}$ mutants but not in wild-type animals (Fig. 3B), suggesting different response thresholds in these genetic backgrounds.

13-EFOX-L_2 levels rise in response to aspirin and LA supplement

The hydroxyl group in 13-HODE, responsible for its chiral nature, can be further oxidized to generate the corresponding electrophilic derivative 13-EFOX-L_2 according to the mechanism proposed by Groeger et al. for other PUFAs (Groeger et al., 2010) (Fig. 3A). We detected 13-EFOX-L_2 in only $hop^{Tum\text{-}l}$ mutants at high aspirin concentrations (1 µM and 1 mM) but not in control animals (Fig. 3C; Fig. S2E). The appearance of 13-EFOX-L_2 correlated with the rise in 13-HODE in response to aspirin treatment of mutants (Fig. 3B), supporting the idea that 13-HODE is a substrate for 13-EFOX-L_2 synthesis *in vivo* (Fig. 3A).

The discovery of 13-HODE and 13-EFOX-L_2, two LA-derived oxylipids, in larval extracts prompted us to examine whether $hop^{Tum\text{-}l}$ mutants would benefit from dietary addition of LA (13-HODE and 13-EFOX-L_2 are chemically not stable enough for such experiments). Addition of 5 mM LA to the diet increased the larval-to-adult viability of $hop^{Tum\text{-}l}$ mutants from 35% to up to 90% while 5 mM myristic acid addition had almost no effect (Fig. S3E).

Unlike 1 µM and 1 mM aspirin, 5 mM LA treatment did not yield a significant increase in 13-HODE (Fig. 3B), but 13-EFOX-L_2 was clearly detected in LA-treated control animals and it was 7-fold higher in LA-treated $hop^{Tum\text{-}l}$ mutants than in their asprin-treated counterparts (Fig. 3C). These correlations suggest that (1) 13-HODE and 13-EFOX-L_2 levels can be modulated by dietary modification in the absence of aspirin, and (2) the *in vivo* effects of aspirin and LA are realized differently. Overall, however, the levels of 13-HODE and 13-EFOX-L_2 correlated with reduced inflammation and improved the survival of $hop^{Tum\text{-}l}$ mutants. We did not detect other members of the EFOX-D or -E families identified in mammalian cells (Groeger et al., 2010) in larval extracts, perhaps because EFOX-D and -E derive from C20 precursors, not found in flies (Shen et al., 2010).

A blood cell-derived signal affects metainflammation and EFOX levels in drug-free $hop^{Tum\text{-}l}$ animals

STAT92E, the sole STAT family member present in flies, acts downstream of Hopscotch, the only Janus kinase found in flies. Previous reports of cell-autonomous effects of $hop^{Tum\text{-}l}$ (Anderson et al., 2017; Hanratty and Ryerse, 1981; Harrison et al., 1995) and the tumor-suppressive property of STAT loss-of-function mutations (Hou et al., 1996; Yan et al., 1996) suggested that STAT KD ($msn{>}STAT^{RNAi}$) in the $hop^{Tum\text{-}l}$ background should relieve tumor burden. We found that tumor penetrance in $hop^{Tum\text{-}l}$ males is significantly reduced with $msn{>}STAT^{RNAi}$ (Fig. 4A), and this reduction may be due, in part, to reduced mitosis in $msn{>}STAT^{RNAi}$ macrophages (Fig. 4B). The *msn* promoter is active in many lymph gland progenitors as early as 56 h (second larval instar; Tokusumi et al., 2009b) and given that the macrophage/lamellocyte lineages have a shared origin (Anderl et al., 2016; Anderson et al., 2017; Stofanko et al., 2010), we hypothesized that mutant blood cells influence the systemic health of animals. Targeted STAT or even *spz* KD ($msn{>}STAT^{RNAi}$ or $msn{>}spz^{RNAi}$) in the hyperplastic $hop^{Tum\text{-}l}$ blood cell population rescued metabolic inflammation in larval adipocytes (Fig. 4C,D), while control RNAi did not (Fig. S2B,C).

This rescue of metabolic inflammation in $hop^{Tum\text{-}l}$ mutants by *STAT* KD suggested a correlative rise in anti-inflammatory oxylipids. We observed an increase in 13-HODE (from 43 nM to 130 nM) and in 13-EFOX-L_2 (from undetectable to 14.0 nM) in an LC-MS/MS quantification of $hop^{Tum\text{-}l}$ $msn{>}STAT^{RNAi}$ animals (Fig. 4E,F). The levels of these oxylipids remained unchanged in control RNAi animals (Fig. S2D,E). These *in vivo* 13-HODE and 13-EFOX-L_2 levels are consistent with corresponding levels in mammalian cells (Groeger et al., 2010; Yuan et al., 2010). Together, our observations suggest that a STAT-dependent pro-inflammatory signal from hematopoietic cells affects immune and metabolic health of flies by regulating 13-HODE and 13-EFOX-L_2 levels.

DISCUSSION

Basic science and clinical discoveries have revealed the pervasive role of inflammation in human disease. Many of these studies expose the intimate links between diet, drugs and disease development (Baker et al., 2011; Hotamisligil, 2006; Serhan et al., 2015; Shapiro et al., 2011). Our studies of the effects of aspirin in fruit flies show that aspirin treatment reduces pro-inflammatory cytokine-producing cells and metabolic inflammation. We further show that these changes correlate with an increase in anti-inflammatory oxylipids.

The anti-mitotic effects of aspirin appear to be important to its salutary effects in flies. In both *Ubc9* and $hop^{Tum\text{-}l}$ flies, *spz* expression is high (Irving et al., 2005; Paddibhatla et al., 2010) and hence the Toll-NF-κB signaling is activated. Thus, selective *spz* KD in $hop^{Tum\text{-}l}$ blood cells improves organismal viability, much as aspirin treatment does. We envision two possible mechanisms of action: (1) aspirin may block the activities of COX-like enzymes (Scarpati et al., 2019; Tootle and Spradling, 2008), which may, in turn, act through the NF-κB/STAT axis in $hop^{Tum\text{-}l}$ blood cells to reduce levels of pro-mitotic/pro-inflammatory proteins, or (2) it may directly block the observed cell cycle progression, for example, by interacting with cell cycle proteins. The anti-mitotic effects of aspirin and reduction in tumorigenesis in flies are consistent with reported salutary effects in epidemiological studies of cancer patients (Elwood et al., 2009; Qiao et al., 2018; Schreinemachers and Everson, 1994). Identifying the direct biochemical targets of aspirin in fly cells (including putative COX enzymes) and understanding its action through these targets will provide new insights into the biochemical effects of aspirin in human cells.

Our biochemical and genetic experiments with the $hop^{Tum\text{-}l}$ larvae revealed the existence of 13-HODE and 13-EFOX-L_2 in flies. Furthermore, these experiments showed that untreated mutants and aspirin-treated mutants differ from the wild-type animals in distinct ways: (1) 13-HODE is detected in untreated *y w* controls and $hop^{Tum\text{-}l}$ mutants; its levels are higher in aspirin-treated controls and $hop^{Tum\text{-}l}$ mutants, as well as in $msn{>}STAT92E$ KD animals; (2) 13-EFOX-L_2 is not detected in untreated control or mutant animals and is found only in aspirin-treated animals or in $msn{>}STAT^{RNAi}$ animals. Because LD morphologies in these mutant animals with high 13-HODE and 13-EFOX-L_2 are restored, we propose that pro-inflammatory signals arising from blood cells adversely affect the metainflammatory state

Journal of Cell Science (2020) 133, jcs236141. doi:10.1242/jcs.236141

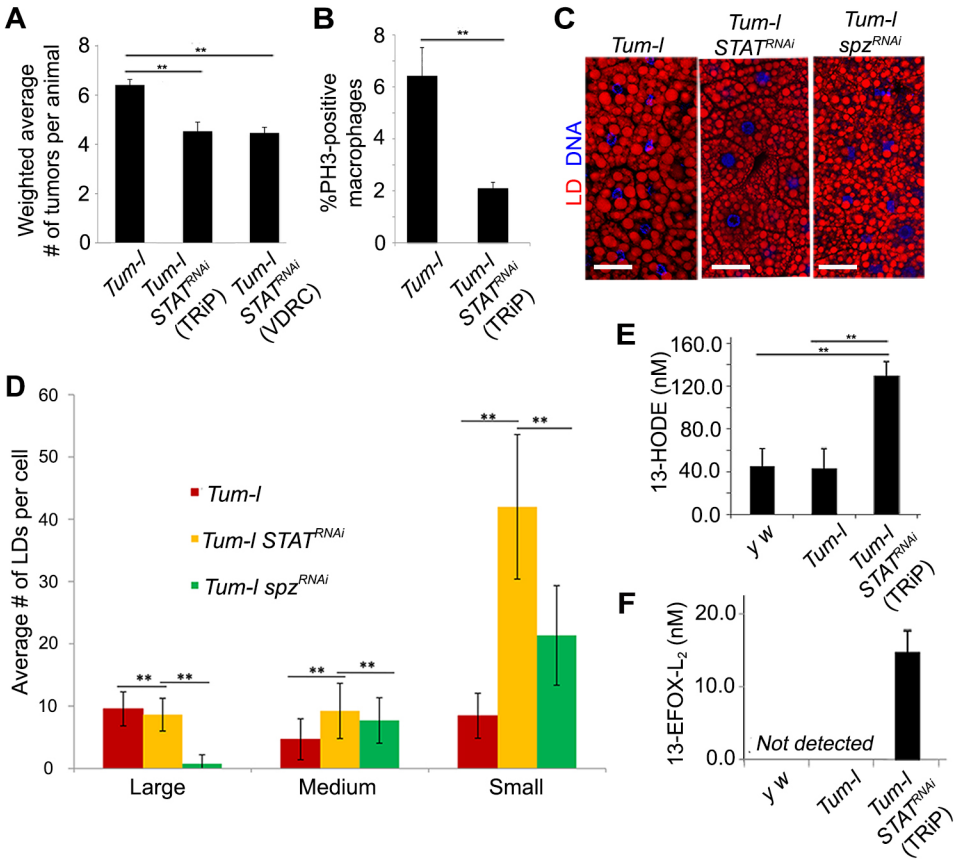

Fig. 4. Immunometabolic crosstalk – a pro-inflammatory signal from macrophages controls systemic levels of 13-HODE and 13-EFOX-L_2 in drug-free animals. (A) Mean±s.e.m. number of tumors (weighted for size, see Materials and Methods) per control (*hop*$^{Tum\text{-}l}$ *msn>mCD8-GFP*) male or per *hop*$^{Tum\text{-}l}$ *msn>mCD8-GFP* male *STAT*^{RNAi} line (27°C). Pairwise comparisons of each experimental class with controls indicate significant differences. ***P*<0.05 (Student's *t*-test). Data from three biological replicates with 28–52 males in each replicate are represented. The total number of tumors observed ranged from 72 to 189. The *P*-values of unweighted average tumor number comparisons (irrespective of size) were also significant (*P*=0.02 and 0.03 for the TRiP and VDRC lines, respectively). (B) Mean±s.e.m. percentage of PH3-positive macrophages in the hemolymph of male larvae is shown. Data were obtained from three biological replicates; hemolymph was examined from 6–10 animals in each replicate. Males were from the *hop*$^{Tum\text{-}l}$ *msn>mCD8-GFP* from *y w* outcross or from the cross with TRiP 31318 females. ***P*<0.05 (Student's *t*-test). (C,D) Nile Red-stained fat bodies from *hop*$^{Tum\text{-}l}$ *msn>mCD8-GFP* without or with *STAT*^{RNAi} or *spz*^{RNAi} expressed in overgrowing blood cells. Average number of large, medium or small LDs per cell from these fat bodies are quantified in D. Bars represent mean±s.d. from three biological replicates, with more than 100 cells per replicate were scored. Three animals per replicate were examined. ***P*<0.001 (Student's *t*-test). (E,F) 13-HODE and 13-EFOX-L_2 levels in larval extracts of control (*y w*) *hop*$^{Tum\text{-}l}$ *msn>mCD8-GFP* without or with *STAT*^{RNAi} (mean±s.d. across four replicates; *n*>200 larvae per replicate). ***P*<0.05 (one-way ANOVA).

of the animal. Reducing such signals results in high levels of 13-HODE and EFOX-L2, reducing metainflammation and improving viability. This interpretation suggests that aspirin treatment of affected mutant flies reverses inflammatory phenotypes by tapping into molecular-genetic pathways that are otherwise inactive in wild-type animals. This suggestion provides new avenues for treating inflammatory diseases, but needs to be substantiated further in flies and other organisms.

How might 13-HODE and 13-EFOX-L_2 work in flies? The chemistry of 13-HODE in mammals may suggest some mechanisms to be explored. The *in vivo* effects of 13-HODE in mammals range from modulating pain sensitivity to affecting metabolic syndrome (Vangaveti et al., 2016). Mammalian 13-HODE serves as a ligand for peroxisome proliferator-activated receptor γ (PPARγ) (Nagy et al., 1998), whose activation alters gene expression and the distribution of surface cell adhesion molecules (Vangaveti et al., 2016). For example, in unchallenged human endothelial cells, 13-HODE and the vitronectin receptor are sequestered in the cytoplasm, but upon interleukin-1 stimulation, the receptor is found on the cell surface, where it mediates endothelial–platelet interaction (Buchanan et al., 1993). We speculate that the differences between adipocyte-macrophage interactions in inflamed and aspirin-treated flies may be mediated by similar changes in cell surface protein composition.

The mode of action of EFOX in mammalian cells appears to be quite different from that of 13-HODE. Half of the cellular EFOX is covalently adducted to proteins, and affects their function. For example, EFOX inhibits the ability of p65, a mammalian NF-κB protein that heterodimerizes with the p50 subunit (encoded by *NFKB1*) (Chen et al., 1998) to bind to DNA (Delmastro-Greenwood et al., 2014; Groeger et al., 2010). Ectopic expression of Dorsal and mouse p50 in flies causes hematopoietic tumors of the kind found in *Ubc9* and *hop*$^{Tum\text{-}l}$ mutants (Govind, 1996). These parallel effects of fly and mouse NF-κB proteins suggest that in flies, as in mammals, 13-EFOX-L_2 can modify protein functions to inactivate immune signaling.

Chronic metabolic and inflammatory disorders together constitute a major health concern worldwide (Ritter and Greten, 2019; Pahwa and Jialal, 2019). The anti-cancer effects of non-steroidal anti-inflammatory drugs (NSAIDs) in humans are not yet well-understood (Gao and Williams, 2012; Hyde and Missailidis,

2009). Aspirin's anti-mitotic and anti-inflammatory effects observed in flies are comparable to its effects in mammals and suggest broad mechanistic similarities in vertebrates and invertebrates. Our work suggests that LA-derived electrophilic fatty acids with anti-inflammatory properties must be also produced in mammalian organs rich in LA. Such a discovery will reinforce the value of the *Drosophila* model system for not only understanding disease progression mechanisms but also for understanding how disease progression (tumor development, dietary stress, and inflammation) can be abated by the animals' intrinsic genetic and biochemical mechanisms.

MATERIALS AND METHODS

Fly lines and crosses

Ubc9 strains (1) *y w; Ubc9$^{4-3}$FRT40A/CyO y^{+}*, (2) *y w; Ubc9^{5} FRT40A/CyO y^{+}*, (3) *y w; Drs-GFP, lwr$^{4-3}$/CyO y^{+}*, and (4) *y w; Drs-GFP lwr^{5}/CyO y^{+}* are described in Chiu et al. (2005). The *76B>GFP* inserts in the *Ubc9* background are described in Kalamarz et al. (2012). The X-linked temperature-sensitive *hop^{Tum-l}* mutation (Luo et al., 1995) was recombined with X-linked *msnf9-GAL4* insert (Tokusumi et al., 2009a). The *mCD8-GFP* reporter transgene [Bloomington *Drosophila* Stock Center (BDSC) no. 5137] was introduced in this background to distinguish macrophages (GFP-negative) from GFP-positive lamellocytes. The final genotype of this stock is: *y w hop^{Tum-l} msn-GAL4/FM7; UAS-mCD8-GFP* and is referred to as *hop^{Tum-l} msn>mCD8-GFP* herein for short.

UAS 'knockdown' lines are as follows. Control *UAS-RNAi* lines used were: *white* [*Drosophila* Transgenic RNAi Project (TRiP) lines 25785 or 28980], *ebony* (TRiP line 28612) and *GFP* (TRiP line 41554). *white* knockdown was validated with the *eyeless-GAL4* driver and *ebony* knockdown was confirmed with universal *daughterless-GAL4* (*da-GAL4*) driver. Loss of the red pigmentation in eyes of *ey>w^{RNAi}* flies and darker adult body color in *da>e^{RNAi}* flies was observed (not shown). The EGFP.shRNA construct was validated in Neumüller et al. (Neumüller et al., 2012).

UAS-STAT^{RNAi} lines used for Signal transducer and activator of transcription (STAT92E) were 31318 (TRiP1), 31317 (TRiP2), and Vienna *Drosophila* Resource Center (VDRC) GD 43867. The TRiP 31318 strain was used for biochemistry. The line for *Spätzle processing enzyme* (*SPE*) knockdown was *w; UAS-SPE^{RNAi}/CyO* (VDRC v30972). For *spätzle* (*spz*) knockdown *y w; UAS-spz^{RNAi}* VDRC v105017 and TRiP 28538 lines were used and for *Toll* (*Tl*) knockdown *UAS-Tl^{RNAi}/MKRS* TRiP 31044 (TRiP1) and 31477 (TRiP2) were used. *UAS-dl^{RNAi}* TRiP (27650) was used for *dorsal* (*dl*) knockdown.

Gene knockdown in *hop^{Tum-l}* flies

Because of the semidominant X-linked mutation, fewer *hop^{Tum-l}/Y* males survive relative to their *FM7/Y* siblings. This genetic background is therefore suitable for biochemical and genetic interaction experiments. *y w hop^{Tum-l} msn-GAL4/FM7; UAS-mCD8-GFP* females were crossed either with *UAS-RNAi* males or with *y w/Y* control males. Effects of RNA interference (*STAT*, *SPE*, *spz*, *Toll* or *dl*) on viability in the *y w hop^{Tum-l} msn-GAL4/FM7; UAS-mCD8-GFP* animals were normalized relative to the *y w* outcross. The proportion of *hop^{Tum-l}/Y* (mutant) sons relative to *FM7/Y* (control) sons is defined as relative rescue. In additional crosses with control *UAS-RNAi* for *white* (two lines), *ebony* or *GFP*, we found that in all four pairwise comparisons, the ratio of surviving *hop^{Tum-l}/Y RNAi* sons relative to *FM7/Y* balancer-carrying sons was statistically indistinguishable from this ratio derived from the *y w/Y* outcross (Fig. S2A).

Chemical treatments

Salicylic acid treatment

SA is the principal metabolite of aspirin and lacks the functional acetyl group characteristic of ASA. SA was dissolved in DMSO to make a 10 M solution. The final DMSO content in the fly food was negligible, being four orders of magnitude lower than the reported cytotoxic DMSO concentration in *Drosophila* larvae (~0.3% w/w; Nazir et al., 2003).

SA treatment of *Ubc9* mutants did not ameliorate tumor penetrance of *Ubc9* mutants. At 1 nM and 50 nM concentrations, all animals (n=10 and n=13, respectively) developed tumors and produced aggregates, much like the untreated controls. None of the mutants was tumor free. This result was also reflected in infiltration indices (number of macrophages adhering to 100 fat body cells) where no significant difference between SA-treated (1.58±0.10 macrophages for 1 nM and 2.46±0.27 macrophages for 50 nM SA, mean±s.e.m.) and control treatment (2.64±0.34 macrophages, no DMSO, or 2.18±0.06 macrophages, with DMSO) was observed (P>0.05). In each case, 100 fat body cells were examined for infiltration by macrophages.

DMSO treatment

No significant difference was observed in tumor penetrance between 'no treatment' or 'DMSO-only' treatment classes of *Ubc9* animals. Under both conditions, all animals developed tumors and/or aggregates. Infiltration index was also statistically indistinguishable (see numbers in the previous section).

Aspirin treatment

The sources of aspirin for *Ubc9* and *hop^{Tum-l}* treatments were different. For *Ubc9* larvae, one 325 mg Bayer aspirin tablet was ground finely and 1 mg/ml of this powder was dissolved in an appropriate amount of water and the suspension was stirred vigorously for 15 min and filtered. An appropriate volume of aspirin solution was added to fly food to yield aspirin concentrations of 0.5 nM or 5.5 µM.

Drug purity in these tablets was determined as follows: A 325 mg tablet was ground to a fine powder and suspended in ice-cold methanol with vigorous stirring for 10 min. It was vacuum-filtered with a Buchner funnel. The solvent was dried under a gentle stream of nitrogen; the white solid powder was further dried under high vacuum, overnight. High purity of the compound (>99.8%) was verified via LC-MS and nuclear magnetic resonance (NMR) analyses. Results matched data reported in the literature (Byrd and Donnell, 2003).

For *hop^{Tum-l}* larvae, a 10 M aspirin (≥99.9%, Sigma-Aldrich) solution in DMSO was diluted in water to achieve a final aspirin concentration of 1 nM, 1 µM or 1 mM in fly food. The final DMSO content in the fly food was significantly lower than levels known to be toxic in *Drosophila* larvae (~0.3% w/w; Nazir et al., 2003). An appropriate volume of the resulting aqueous solution was added directly to fly food and thoroughly homogenized with an electric mixer for 15 min. Larvae were reared at 27°C and collected for lipid extraction, viability assays, or dissections, 5 days after egg laying, unless stated otherwise.

Viability of 0.5 nM and 5.5 µM aspirin-treated *y w* animals remained as high as untreated *y w* animals (98–100%) and no toxic effects were observed, whereas addition of 1 mM aspirin in fly food resulted in partial lethality at pupal stages. Aspirin administration did not rescue recessive lethality of *Ubc9* mutants. To examine the effects of aspirin on larval-to-adult viability, the number of *hop^{Tum-l} msn>mCD8-GFP* adults emerging from a known number of second- and third-instar larvae (untreated or treated with 1 nM, 1 µM, or 1 mM of aspirin) was scored.

Linoleic acid and myristic acid treatment

An appropriate volume of pure LA (≥99.9%, Sigma-Aldrich) was added directly to fly food for a final concentration of 5 mM. The mixture was homogenized into fly food for 15 min. *y w* and *hop^{Tum-l} msn>mCD8-GFP* larvae were reared at 27°C for 5 days and collected for lipid extraction or viability assays. Myristic acid (MA,≥99.9%, Sigma-Aldrich) was similarly administered, also at 5 mM final concentration.

Synthesis of Rhodamine B-conjugated aspirin and visualization

In a 150 ml two-neck round bottom flask, 2 g (4 mmol) of Rhodamine B was dissolved in 16 ml (10 mmol, 2.5 equivalent) of phosphoryl chloride ($POCl_3$) and the mixture was vigorously stirred at 110°C for 2 days. Subsequently, $POCl_3$ was thoroughly distilled off under vacuum after which 60 ml of molecular sieve-dried acetonitrile was added to the flask along with 2.1 g (11.3 mmol, 2.8 equivalent) of mono-Boc-protected piperazine and 0.7 ml (5 mmol, 1.2 equivalent) of triethylamine. The mixture was stirred at room temperature for 24 h, and then for 12 h under reflux. Once thin layer chromatography showed complete conversion of the starting material,

Journal of Cell Science (2020) 133, jcs236141. doi:10.1242/jcs.236141

triethylamine was distilled off and the crude product was dissolved in 20 ml of trifluoroacetic acid and stirred for 2 h at room temperature. The solvent was removed and the crude product was purified via flash chromatography (the initial eluting mixture 5.5:1 $CHCl_3$:CH_3OH changed gradually to a 2:1 ratio). After collecting the correct fractions, the solvent was removed using a rotary evaporator and the final product was precipitated by dissolving it in 2 ml of methanol and then adding it to 50 ml of diethyl ether, drop-wise.

After drying it under vacuum, 150 mg of this intermediate (1 equivalent) was dissolved in 10 ml of DMSO to which 54 mg of aspirin (0.3 mmol, 1 equivalent), 153 µl of triethylamine and 410 mg of HBTU (1 mmol, 3.3 equivalent) were added in this order. The mixture was stirred for 24 h at room temperature under nitrogen. At the end of this period, 150 ml of 0.5 M sodium bicarbonate ($NaHCO_3$) were added, followed by 100 ml of ethyl acetate. The biphasic mixture was transferred into a separatory funnel. Upon vigorous stirring, the organic phase was recovered, whereas the aqueous phase was extracted three times with ethyl acetate. The combined organic fractions were dried over Na_2SO_4. After filtration on a cotton plug, the solvent was removed by rotary evaporator almost to dryness. The crude product was dissolved in 2 ml of ethyl acetate, which was added to 150 ml of diethyl ether drop-wise at room temperature. After keeping the solution at 4°C for 1 h, the product was recovered via filtration and dried in vacuum to yield 160 mg of Rhodamine B-conjugated aspirin {Rh-ASA, 80% yield over two steps; 1H-NMR: 400 MHz, δ (ppm): 1.13 (12H, t), 2.08 (3H, s), 3.39 (12H, q), 3.50 (4H, t), 3.60 (4H, t), 5.34 (1H, d), 6.13 (2H, s), 6.19 (2H, d), 6.84 (2H, dd), 7.24 (1H, s), 7.25 (3H), 7.39 (1H), 7.48 (1H, dd), 7.83 (1H, d), 7.92 (1H, d); MS: $[M\text{-}Cl^-]^+$=444.24 *m*/*z*}. A working solution [800 µM Rh-ASA in phosphate-buffered saline (PBS, pH 7.2)] was applied to dissected larval tissues for 30 min at room temperature in a humidified chamber. Negative control samples were exposed to a mixture of 800 µM Rhodamine B plus 800 µM aspirin solution in PBS.

Analysis of aspirin-treated animals

Tumor penetrance and expressivity

The effects of aspirin on the presence and abundance of tumors (penetrance) and tumor sizes (expressivity) were scored in 8-day-old *Ubc9* animals. Age-matched third-instar heterozygous or mutant *Ubc9* larvae were chosen without bias to sex from a timed (6–24 h) egg lay. Developmentally delayed larvae (smaller in size than majority of mutants) were not selected for analysis. In three independent experiments, all available mutant untreated or aspirin-treated animals were first scored for the absence/presence of visible tumors using a stereomicroscope. All animals were then dissected and all tumors were mounted on slides and imaged with a Zeiss Axioscope 2 Plus microscope. Surface area measurements (a measure of tumor size) were made using the AxioVision LE 4.5 software. Because of the recessive lethality of the mutation, few mutants survive at 8 days.

Dissection and immunostaining

Fat bodies, lymph glands, blood cell smears or tumors were dissected from *y w*, heterozygous or mutant larvae (Kalamarz et al., 2012; Small et al., 2012). Air-dried blood cells, aggregates and tumor samples were stained according to protocols described in Paddibhatla et al. (2010) and Small et al. (2012). Samples were mounted in either 70–80% glycerol or in Vectashield (Vector Labs) and were imaged with a Zeiss 510 or 710 laser scanning confocal microscope and formatted in Zeiss LSM5 or Zen 2.3 software.

Tumor and lymph gland lobe size

Larval tumors

For frequency and size of blood tumors, age-matched *Ubc9* larvae were collected 8 days after egg laying. Washed animals were bled, and hemolymph contents were recovered on glass slides and air-dried, fixed in 4% paraformaldehyde in PBS (pH 7.2), mounted in 80% glycerol and photographed using a CCD camera on a Zeiss Axioscope. AxioVision LE Rel. 4.5 software was used to measure projection areas. This term refers to the area internal to the outline of a fixed, mounted and imaged structure. Structures smaller than 10,000 µm^2 in projection areas were recorded as aggregates and are not reported, while those larger than 10,000 µm^2 were defined as microtumors or tumors (Kalamarz et al., 2012). Treatment labels on slides were masked to remove bias during measurement and analysis (single-blind analysis).

Lymph gland lobe size

The projection areas of individual anterior and first set of larva posterior lobes (of the same gland) from age-matched, untreated or 0.5 nM aspirin-treated 6-day-old larvae were measured in the same way as tumors and aggregates above.

Tumors in adult flies

All tumors in dorsal and ventral abdominal areas were scored for (1) $hop^{Tum\text{-}l}$ *msn>mCD8-GFP* males (from a cross of $hop^{Tum\text{-}l}$ *msn-GAL4/FM7; UAS-mCD8-GFP* females with *y w/Y* males) and (2) $hop^{Tum\text{-}l}$ *msn-GAL4/Y; UAS-mCD8-GFP* males, expressing $STAT^{RNAi}$ (lines VDRC GD 43867 or TRiP line 31318), cultured at 27°C. A tumor was considered small if it was less than half the length of the body segment, medium-sized if it spanned more than half but less than a complete body segment, and large if the surface area of the tumor exceeded one entire segment. A medium and large tumor was weighted to equal two or three small tumors, respectively. The average number of tumors (weighted for size in this way) was computed for each cross and pairwise comparisons of average number of tumors/animal in each experimental class with a control class were made to determine differences due to $STAT^{RNAi}$ expression. Larval hemolymph was examined for mitotic index (see below).

Mitosis

For scoring the mitotic index in $hop^{Tum\text{-}l}$ *msn>mCD8-GFP* blood cells (without or with aspirin), rabbit anti-PH3 (1:200; Cat #06-570, Lot #2465253, EMD Millipore) antibody was visualized with anti-rabbit alkaline phosphatase-linked secondary antibody (1:5000; Product #31340, Lot #Q5226802, Thermo Fisher Scientific). Alkaline phosphatase staining was performed with 125 µg/ml BCIP and 250 µg/ml NBT from Promega. Mitotic indices of control $hop^{Tum\text{-}l}$ *msn>mCD8-GFP* larvae (from *y w* crosses) and $hop^{Tum\text{-}l}$ *msn>mCD8-GFP* animals expressing $STAT^{RNAi}$ (TRiP 31318) were determined using the same methods, except that blood cells from only male larvae were examined in each case.

Reporter gene expression

Changes in *Drs-GFP* expression in third-instar larval fat bodies were assessed at 6 days and 8 days after egg laying. The entire fat body was carefully dissected and mounted on a slide. The status of GFP expression in the organ was scored under a Zeiss Axioplan 2. AxioVision LE 4.5 software was used to process images.

Infiltration index

Third-instar larval fat bodies were dissected from untreated control and aspirin-treated larvae. Dissected tissues were fixed and stained with Hoechst 33258 and TRITC-labeled phalloidin. Samples were mounted in 50% glycerol in PBS (pH 7.4). The number of single blood cells adhering above or below the fat body were scored as described in Paddibhatla et al. (2010) under a Zeiss Axioscope fluorescence microscope.

Slide preparation for fat body lipid droplet analysis

Fat body LDs were detected after fixation and staining with Nile Red (N3013, Sigma-Aldrich) as described by Greenspan et al. (1985). Samples were kept in PBS (pH 7.2) throughout the procedure. Samples were counterstained with the nuclear dye Hoechst 33258 and were mounted in Vectashield (both from Invitrogen Molecular Probes). To preserve the endogenous LD sizes, slides carrying fat body samples were prepared as follows. Fixed, Nile Red- and Hoechst 33258-stained fat body pieces were mounted on slides with a spacer to prevent distortion of LDs and maintain normal tissue morphology. (1) A 4–5-cm strip of single-sided Scotch tape was placed in the center of the slide. (2) A thin, even layer of Vaseline was applied onto the tape with a paintbrush. (3) Using the corner of a razor blade, a 1 cm×3 cm rectangle was excised from the tape and peeled off using tweezers. (The exposed rectangular area becomes the well for the sample.) (4) A drop of Vectashield was placed in the well and evenly spread on the glass surface. (5) Using clean tweezers, three to four pieces of the stained fat

bodies (in PBS, pH 7.4) were transferred into the well, avoiding overlap. (6) A glass cover slip was then gently placed over the samples and uniformly pressed; the Vaseline adheres the tape to the coverslip. The sample in the Vectashield should now occupy the well. (7) Clear nail polish was gently applied to seal the coverslip. While the prepared slides can be stored at 4°C, optimal results were obtained when samples were imaged immediately. Samples were imaged on a Zeiss LSM 510 or 710 confocal microscope. LD sizes were classified as follows: small [radius (r)<3.1 µm]; medium (3.1<r<5 µm); large (r>5 µm).

Biochemistry

For oxidized lipids in *Drosophila* larvae, we used solid-phase extraction methods (Massey and Nicolaou, 2013). At least 200 age-matched animals were transferred from fly food onto a fine-sieve mesh, washed with water, then 70% ethanol, and then again with water, and gently dried with a Kimwipe. Samples were weighed and stored at −80°C until further use.

Materials for lipidomics

Materials used were as follows. Solid-phase extraction STRATA SPE cartridges: C18-E (500 mg, 6 ml; Cat. No. 8B-S001-HCH); non-chiral RP-HPLC column: Phenomenex Luna 3 µm C18(2) 100A 150×2.0 mm; Chiral HPLC column: Chiracel OD-RH 5 µm 150×2.1 mm; MS system: 4000 QTRAP (Applied Biosystems), HPLC system: Shimadzu Prominence HPLC (Shimadzu USA); NMR instrument: Varian Mercury-300. MS-grade water, acetonitrile and formic acid were purchased from WorldWide Life Sciences (Bristol, PA). The following analytical-grade standards were purchased from Cayman Chemical Co. (Ann Arbor, MI): 13(S)-HODE (>98%), 13-EFOX-L_2 (>98%), 13(S)-HOTrE (>98%), 13(S)-HODE-d_4 (>99% deuterated), 13-EFOX-L_2-d_3 (>99% deuterated).

Sample preparation

The amounts of solvents and internal standards before solid-phase extraction used for 200 mg of larvae are presented below; these amounts were adjusted where larval weight exceeded 200 mg. For lipid extraction, larvae were transferred into a 1 ml pre-chilled glass Dounce grinder and homogenized thoroughly at 0°C with a glass pestle along with 500 µl of cold methanol. The pestle was rinsed twice with 100 µl of cold methanol. 4 ml of ice-cold was were added to obtain a 15% methanol solution. Subsequently, 50 ng of deuterated internal standards were added to the homogenate, which was left on ice in the dark. After 15 min the homogenate was centrifuged at 4°C and 3,700 ***g*** for 10 min. The supernatant was recovered and kept on ice. The pH was then adjusted to 3 by adding 10–20 drops of 0.1 M HCl and 2.00 ml of the acidic extract were immediately loaded onto the SPE column, which was previously conditioned with 20 ml of methanol and 20 ml of water. The cartridge was washed with 20 ml of ice-cold 15% methanol in water, 20 ml of water and 10 ml of hexane. The lipids were recovered with 12 ml of cold methyl formate, which was evaporated on ice and in the dark under a gentle stream of nitrogen. The purified lipids were dissolved in 1 ml of cold degassed ethanol, and stored at −80°C until the LC-MS analysis.

Lipid derivatives were analyzed on a reverse phase-high pressure liquid chromatography coupled to a mass spectrometer (RP-HPLC MS/MS). The non-chiral LC-MS runs were performed after diluting the extract 10-fold in ethanol. All samples were analyzed with a gradient solvent system consisting of A (water with 0.1% formic acid) and B (acetonitrile with 0.1% formic acid). The flow rate was 250 µl/min and the gradient used was the following: hold at 35% B for 3 min, then 35–90% B in 23 min, then 90–100% B in 0.1 min, hold for 5.9 min and 100–35% B in 0.1 min, and finally hold for 7.9 min. The oven temperature was 40°C. Chiral analyses were performed in isocratic elution with 35% A and 65% B for 25 min. The flow rate was 250 µl/min and the oven temperature was 40°C.

LC-MS analyses were performed in Multiple Reaction Monitoring (MRM) mode whose optimal parameters and most-abundant fragments were obtained experimentally for 13-HOTrE, 13-HODE and 13-EFOX-L_2 by utilizing commercially available synthetic standards. The settings used are shown in Table S1. Standard curves were prepared using 13-HODE and 13-EFOX-L_2 as analytes and 13-HODE-d_4 and 13-EFOX-L_2-d_3 as internal standards. Analyte:internal standard peak area ratios were used for quantification. Comparison of retention times and the use of at least two MS transitions per compound rendered the detection reliable and sensitive (Fig. S3B,C and Fig. S4). Data were analyzed by one-way ANOVA.

Statistical analysis

Experiments were replicated three or more times. Where results were quantified, at least three biological repeats were performed. The numbers of animals tested are indicated in the text or in the Figure legend. For pairwise comparison, either one-way ANOVA or the t-test was applied. P<0.05 was considered to be significant.

Acknowledgements

The Mott Hall Middle School students, F. Lopez and D. Mendia helped initiate this project. We thank Govind lab members M. J. Lee, L. H. Huang, Z. Huda, and Z. Papadopol for help with experiments and feedback. We are grateful to R. A. Schulz, Bloomington *Drosophila* Stock Center, and VDRC for fly strains. K. Dastmalchi provided suggestions on lipidomics experiments, L. Yang provided technical support for mass spectrometry, and S. G. Wendell provided critical input on the manuscript.

Competing interests

The authors declare no competing or financial interests.

Author contributions

Conceptualization: S.P., I.P., J.C., R.R., R.S.M., T.G., G.J., S.G.; Methodology: S.P., J.C., R.R., R.S.M., T.G., S.G.; Validation: S.P., I.P., J.C., R.R., R.S.M., T.G., S.G.; Formal analysis: S.P., I.P., J.C., R.R., R.S.M., T.G., S.G.; Investigation: S.P., I.P., J.C., R.R., R.S.M., T.G., S.G.; Resources: S.G.; Data curation: S.P., J.C., R.R., R.S.M., T.G., S.G.; Writing - original draft: S.P., S.G.; Writing - review & editing: S.P., I.P., J.C., R.R., R.S.M., S.G.; Visualization: S.P., I.P., J.C., S.G.; Supervision: S.G.; Project administration: S.G.; Funding acquisition: G.J., S.G.

Funding

This work was supported by funds from the National Science Foundation (1121817-SG and 1512458-GJ), National Aeronautics and Space Administration (NASA) (NNX15AB42G-SG), and the National Institutes of Health (S06 GM08168, 8G12MD007603-30-RCMI). Deposited in PMC for release after 12 months.

Supplementary information

Supplementary information available online at
http://jcs.biologists.org/lookup/doi/10.1242/jcs.236141.supplemental

References

Alfonso, L., Ai, G., Spitale, R. C. and Bhat, G. J. (2014). Molecular targets of aspirin and cancer prevention. *Br. J. Cancer* **111**, 61-67. doi:10.1038/bjc.2014.271

Anderl, I., Vesala, L., Ihalainen, T. O., Vanha-aho, L.-M., Andó, I., Rämet, M. and Hultmark, D. (2016). Transdifferentiation and proliferation in two distinct hemocyte lineages in drosophila melanogaster larvae after wasp infection. *PLoS Pathog.* **12**, e1005746. doi:10.1371/journal.ppat.1005746

Anderson, A. M., Bailetti, A. A., Rodkin, E., De, A. and Bach, E. A. (2017). A genetic screen reveals an unexpected role for yorkie signaling in jak/stat-dependent hematopoietic malignancies in drosophila melanogaster. *G3 (Bethesda)* **7**, 2427-2438. doi:10.1534/g3.117.044172

Baker, R. G., Hayden, M. S. and Ghosh, S. (2011). NF-κB, inflammation and metabolic disease. *Cell Metab.* **13**, 11-22. doi:10.1016/j.cmet.2010.12.008

Bozza, P. T., Payne, J. L., Morham, S. G., Langenbach, R., Smithies, O. and Weller, P. F. (1996). Leukocyte lipid body formation and eicosanoid generation: cyclooxygenase-independent inhibition by aspirin. *Proc. Natl. Acad. Sci. USA* **93**, 11091-11096. doi:10.1073/pnas.93.20.11091

Buchanan, M., Bertomeu, M., Haas, T., Orr, F. and Eltringham-Smith, L. (1993). Localization of 13-hydroxyoctadecadienoic acid and the vitronectin receptor in human endothelial cells and endothelial cell/platelet interactions in vitro. *Blood* **81**, 3303-3312.

Byrd, H. and Donnell, S. E. O. (2003). A general chemistry laboratory theme: spectroscopic analysis of aspirin. *J. Chem. Educ.* **80**, 174. doi:10.1021/ed080p174

Chen, F. E., Huang, D.-B., Chen, Y.-Q. and Ghosh, G. (1998). Crystal structure of p50/p65 heterodimer of transcription factor nf-[kappa]b bound to DNA. *Nature* **391**, 410-413. doi:10.1038/34956

Cherry, S. and Silverman, N. (2006). Host-pathogen interactions in drosophila: new tricks from an old friend. *Nat. Immunol.* **7**, 911-917. doi:10.1038/ni1388

Chiu, H., Ring, B. C., Sorrentino, R. P., Kalamarz, M., Garza, D. and Govind, S. (2005). dUbc9 negatively regulates the Toll-NF-kappa B pathways in larval hematopoiesis and drosomycin activation in Drosophila. *Dev. Biol.* **288**, 60-72. doi:10.1016/j.ydbio.2005.08.008

Cressler, C. E., Nelson, W. A., Day, T. and McCauley, E. (2014). Disentangling the interaction among host resources, the immune system and pathogens. *Ecol. Lett.* **17**, 284-293. doi:10.1111/ele.12229

Delmastro-Greenwood, M., Freeman, B. A. and Wendell, S. G. (2014). Redox-dependent anti-inflammatory signaling actions of unsaturated fatty acids. *Annu. Rev. Physiol.* **76**, 79-105. doi:10.1146/annurev-physiol-021113-170341

Dennis, E. A. and Norris, P. C. (2015). Eicosanoid storm in infection and inflammation. *Nat. Rev. Immunol.* **15**, 511-523. doi:10.1038/nri3859

Elwood, P. C., Gallagher, A. M., Duthie, G. G., Mur, L. A. J. and Morgan, G. (2009). Aspirin, salicylates, and cancer. *Lancet* **373**, 1301-1309. doi:10.1016/S0140-6736(09)60243-9

Gao, L. I. and Williams, J. L. (2012). Nitric oxide-donating aspirin induces g(2)/m phase cell cycle arrest in human cancer cells by regulating phase transition proteins. *Int. J. Oncol.* **41**, 325-330. doi:10.3892/ijo.2012.1455

Govind, S. (1996). Rel signalling pathway and the melanotic tumour phenotype of Drosophila. *Biochem. Soc. Trans.* **24**, 39-44. doi:10.1042/bst0240039

Govind, S. (2008). Innate immunity in Drosophila: pathogens and pathways. *Insect Sci.* **15**, 29-43. doi:10.1111/j.1744-7917.2008.00185.x

Govind, S. and Nehm, R. H. (2004). Innate immunity in fruit flies: a textbook example of genomic recycling. *PLoS Biol.* **2**, E276. doi:10.1371/journal.pbio.0020276

Greenspan, P., Mayer, E. P. and Fowler, S. D. (1985). Nile red: a selective fluorescent stain for intracellular lipid droplets. *J. Cell Biol.* **100**, 965-973. doi:10.1083/jcb.100.3.965

Gregor, M. F. and Hotamisligil, G. S. (2011). Inflammatory mechanisms in obesity. *Annu. Rev. Immunol.* **29**, 415-445. doi:10.1146/annurev-immunol-031210-101322

Groeger, A. L., Cipollina, C., Cole, M. P., Woodcock, S. R., Bonacci, G., Rudolph, T. K., Rudolph, V., Freeman, B. A. and Schopfer, F. J. (2010). Cyclooxygenase-2 generates anti-inflammatory mediators from omega-3 fatty acids. *Nat. Chem. Biol.* **6**, 433-441. doi:10.1038/nchembio.367

Hanratty, W. P. and Ryerse, J. S. (1981). A genetic melanotic neoplasm of drosophila melanogaster. *Dev. Biol.* **83**, 238-249. doi:10.1016/0012-1606(81)90470-X

Harrison, D. A., Binari, R., Nahreini, T. S., Gilman, M. and Perrimon, N. (1995). Activation of a Drosophila Janus kinase (JAK) causes hematopoietic neoplasia and developmental defects. *EMBO J.* **14**, 2857-2865. doi:10.1002/j.1460-2075.1995.tb07285.x

Hotamisligil, G. S. (2006). Inflammation and metabolic disorders. *Nature* **444**, 860-867. doi:10.1038/nature05485

Hou, X. S., Melnick, M. B. and Perrimon, N. (1996). Marelle acts downstream of the drosophila hop/jak kinase and encodes a protein similar to the mammalian stats. *Cell* **84**, 411-419. doi:10.1016/S0092-8674(00)81286-6

Hyde, C. A. C. and Missailidis, S. (2009). Inhibition of arachidonic acid metabolism and its implication on cell proliferation and tumour-angiogenesis. *Int. Immunopharmacol.* **9**, 701-715. doi:10.1016/j.intimp.2009.02.003

Irving, P., Ubeda, J.-M., Doucet, D., Troxler, L., Lagueux, M., Zachary, D., Hoffmann, J. A., Hetru, C. and Meister, M. (2005). New insights into Drosophila larval haemocyte functions through genome-wide analysis. *Cell. Microbiol.* **7**, 335-350. doi:10.1111/j.1462-5822.2004.00462.x

Kalamarz, M. E., Paddibhatla, I., Nadar, C. and Govind, S. (2012). Sumoylation is tumor-suppressive and confers proliferative quiescence to hematopoietic progenitors in Drosophila melanogaster larvae. *Biol. Open* **1**, 161-172. doi:10.1242/bio.2011043

Kim, M. J. and Choe, K.-M. (2014). Basement membrane and cell integrity of self-tissues in maintaining Drosophila immunological tolerance. *PLoS Genet.* **10**, e1004683. doi:10.1371/journal.pgen.1004683

Kopp, E. and Ghosh, S. (1994). Inhibition of NF-kappa B by sodium salicylate and aspirin. *Science* **265**, 956. doi:10.1126/science.8052854

Lawrence, T. (2009). The nuclear factor nf-κb pathway in inflammation. *Cold Spring Harbor Perspect. Biol.* **1**, a001651. doi:10.1101/cshperspect.a001651

Lee, J. Y., Sohn, K. H., Rhee, S. H. and Hwang, D. (2001). Saturated fatty acids, but not unsaturated fatty acids, induce the expression of cyclooxygenase-2 mediated through Toll-like receptor 4. *J. Biol. Chem.* **276**, 16683-16689. doi:10.1074/jbc.M011695200

Lee, J. Y., Ye, J., Gao, Z., Youn, H. S., Lee, W. H., Zhao, L., Sizemore, N. and Hwang, D. H. (2003). Rmodulation of toll-like receptor-4 signaling pathways involving myd88 and phosphatidylinositol 3-kinase/akt by saturated and polyunsaturated fatty acids. *J. Biol. Chem.* **278**, 37041-37051. doi:10.1074/jbc.M305213200

Lemaitre, B. and Hoffmann, J. (2007). The host defense of Drosophila melanogaster. *Annu. Rev. Immunol.* **25**, 697-743. doi:10.1146/annurev.immunol.25.022106.141615

Luo, H., Hanratty, W. P. and Dearolf, C. R. (1995). An amino acid substitution in the Drosophila hopTum-l Jak kinase causes leukemia-like hematopoietic defects. *EMBO J.* **14**, 1412-1420. doi:10.1002/j.1460-2075.1995.tb07127.x

Massey, K. A. and Nicolaou, A. (2013). Lipidomics of oxidized polyunsaturated fatty acids. *Free Radic. Biol. Med.* **59**, 45-55. doi:10.1016/j.freeradbiomed.2012.08.565

Musselman, L. P., Fink, J. L., Narzinski, K., Ramachandran, P. V., Hathiramani, S. S., Cagan, R. L. and Baranski, T. J. (2011). A high-sugar diet produces obesity and insulin resistance in wild-type drosophila. *Dis. Models Mech.* **4**, 842-849. doi:10.1242/dmm.007948

Nagy, L., Tontonoz, P., Alvarez, J. G. A., Chen, H. and Evans, R. M. (1998). Oxidized LDL regulates macrophage gene expression through ligand activation of PPAR-gamma. *Cell* **93**, 229-240. doi:10.1016/S0092-8674(00)81574-3

Nazir, A., Mukhopadhyay, I., Saxena, D. K. and Chowdhuri, D. K. (2003). Evaluation of the No observed adverse effect level of solvent dimethyl sulfoxide in Drosophila melanogaster. *Toxicol. Mech. Methods* **13**, 147-152. doi:10.1080/15376510309846

Neumüller, R. A., Wirtz-Peitz, F., Lee, S., Kwon, Y., Buckner, M., Hoskins, R. A., Venken, K. J. T., Bellen, H. J., Mohr, S. E. and Perrimon, N. (2012). Stringent analysis of gene function and protein–protein interactions using fluorescently tagged genes. *Genetics* **190**, 931-940. doi:10.1534/genetics.111.136465

Paddibhatla, I., Lee, M. J., Kalamarz, M. E., Ferrarese, R. and Govind, S. (2010). Role for sumoylation in systemic inflammation and immune homeostasis in Drosophila larvae. *PLoS Pathog.* **6**, e1001234. doi:10.1371/journal.ppat.1001234

Pahwa, R. and Jialal, I. (2019). *Chronic Inflammation*. StatPearls Publishing. https://www.ncbi.nlm.nih.gov/books/NBK507799/

Qiao, Y., Yang, T., Gan, Y., Li, W., Wang, C., Gong, Y. and Lu, Z. (2018). Associations between aspirin use and the risk of cancers: a meta-analysis of observational studies. *BMC Cancer* **18**, 288. doi:10.1186/s12885-018-4156-5

Ritter, B. and Greten, F. R. (2019). Modulating inflammation for cancer therapy. *J. Exp Med.* **216**, 1234-1243. doi:10.1084/jem.20181739

Scarpati, M., Qi, Y., Govind, S. and Singh, S. (2019). A combined computational strategy of sequence and structural analysis predicts the existence of a functional eicosanoid pathway in Drosophila melanogaster. *PLoS ONE* **14**, e0211897. doi:10.1371/journal.pone.0211897

Schreinemachers, D. M. and Everson, R. B. (1994). Aspirin use and lung, colon, and breast cancer incidence in a prospective study. *Epidemiology* **5**, 138-146. doi:10.1097/00001648-199403000-00003

Serhan, C. N., Chiang, N. and Dalli, J. (2015). the resolution code of acute inflammation: novel pro-resolving lipid mediators in resolution. *Semin. Immunol.* **27**, 200-215. doi:10.1016/j.smim.2015.03.004

Shapiro, H., Lutaty, A. and Ariel, A. (2011). Macrophages, meta-inflammation, and immuno-metabolism. *TheScientificWorldJOURNAL* **11**, 21. doi:10.1100/2011/397971

Shen, L. R., Lai, C. Q., Feng, X., Parnell, L. D., Wan, J. B., Wang, J. D., Li, D., Ordovas, J. M. and Kang, J. X. (2010). Drosophila lacks c20 and c22 pufas. *J. Lipid Res.* **51**, 2985-2992. doi:10.1194/jlr.M008524

Small, C., Paddibhatla, I., Rajwani, R. and Govind, S. (2012). An introduction to parasitic wasps of Drosophila and the antiparasite immune response. *J. Vis. Exp.* **63**, e3347. doi:10.3791/3347

Stofanko, M., Kwon, S. Y. and Badenhorst, P. (2010). Lineage tracing of lamellocytes demonstrates drosophila macrophage plasticity. *PLoS ONE* **5**, e14051. doi:10.1371/journal.pone.0014051

Tan, L., Xin, X., Zhai, L. and Shen, L. (2016). Drosophila fed ARA and EPA yields eicosanoids, 15S-hydroxy-5Z,8Z, 11Z, 13E-eicosatetraenoic acid, and 15S-hydroxy-5Z,8Z,11Z,13E,17Z-eicosapentaenoic acid. *Lipids* **51**, 435-449. doi:10.1007/s11745-016-4131-3

Tokusumi, T., Shoue, D. A., Tokusumi, Y., Stoller, J. R. and Schulz, R. A. (2009a). New hemocyte-specific enhancer-reporter transgenes for the analysis of hematopoiesis in Drosophila. *Genesis* **47**, 771-774. doi:10.1002/dvg.20561

Tokusumi, T., Sorrentino, R. P., Russell, M., Ferrarese, R., Govind, S. and Schulz, R. A. (2009b). Characterization of a lamellocyte transcriptional enhancer located within the misshapen gene of drosophila melanogaster. *PLoS ONE* **4**, e6429. doi:10.1371/journal.pone.0006429

Tootle, T. L. and Spradling, A. C. (2008). Drosophila pxt: a cyclooxygenase-like facilitator of follicle maturation. *Development (Cambridge, England)* **135**, 839. doi:10.1242/dev.017590

Vangaveti, V. N., Jansen, H., Kennedy, R. L. and Malabu, U. H. (2016). Hydroxyoctadecadienoic acids: oxidised derivatives of linoleic acid and their role in inflammation associated with metabolic syndrome and cancer. *Eur. J. Pharmacol.* **785**, 70-76. doi:10.1016/j.ejphar.2015.03.096

Yan, R., Luo, H., Darnell, J. E. and Dearolf, C. R. (1996). A jak-stat pathway regulates wing vein formation in drosophila. *Proc. Natl. Acad. Sci. USA* **93**, 5842-5847. doi:10.1073/pnas.93.12.5842

Yuan, H., Li, M.-Y., Ma, L. T., Hsin, M. K. Y., Mok, T. S. K., Underwood, M. J. and Chen, G. G. (2010). 15-lipoxygenases and its metabolites 15(S)-HETE and 13(S)-HODE in the development of non-small cell lung cancer. *Thorax* **65**, 321-326. doi:10.1136/thx.2009.122747

Figure S1

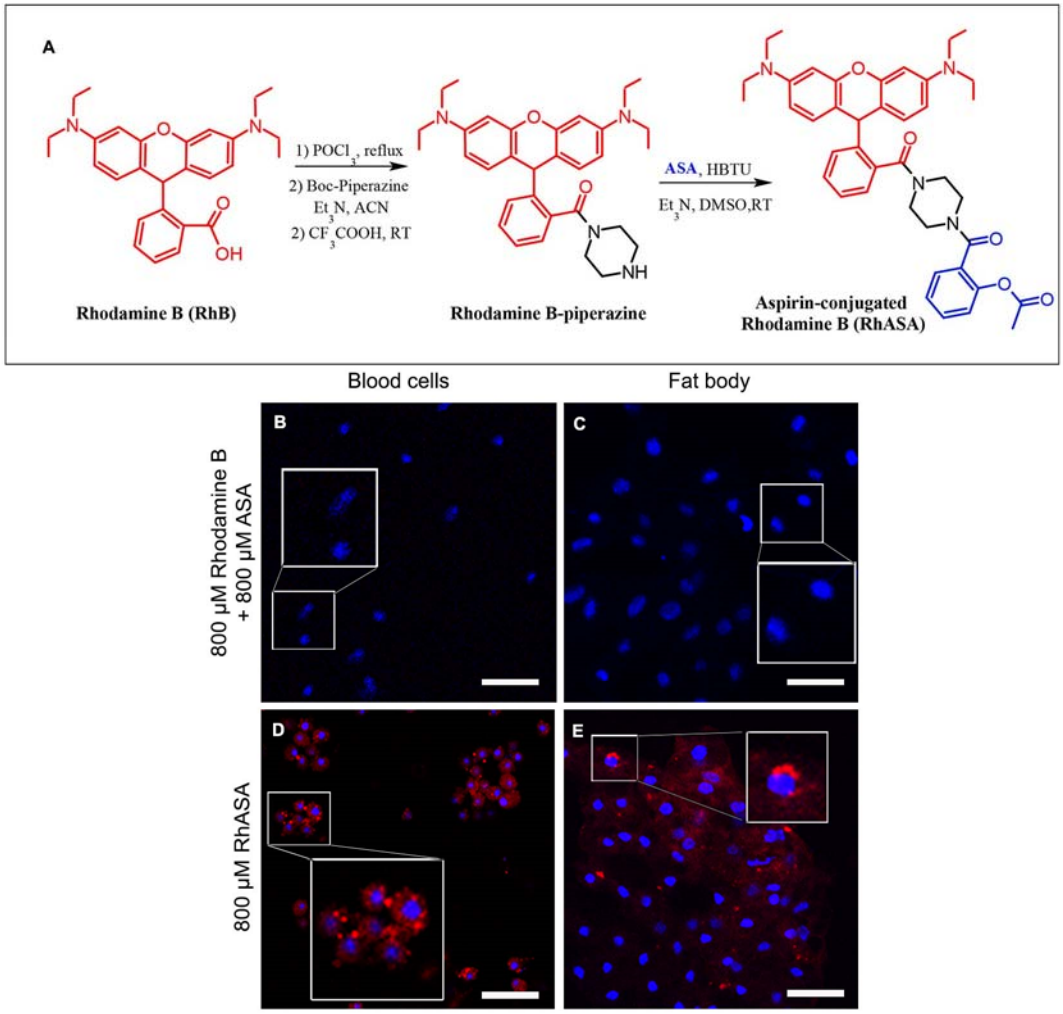

Fig. S1. Aspirin uptake by fly cells. (A) Synthesis of Rhodamine B-labeled aspirin. Rhodamine B was first mono-amidated with piperazine. Then, the carboxylic acid moiety of aspirin was conjugated to the secondary amine in the piperazine moiety. RT refers to room temperature.
(B-E) Incubation of live *Ubc9*$^{-/-}$ larval tissues with unconjugated Rh and free aspirin (B, C), or 800 µM aspirin-conjugated Rhodamine B (RhASA; D, E). Uptake in circulating blood cells (B, D) and fat body adipocytes (C, E) is shown. Unconjugated Rh is not retained but subcellular localization of RhASA is clearly observed (C and E). Cells were counterstained with Hoechst 33258 after fixation. Scale bars show 15 µm (B & D), and 50 µm (C & E). Cells in the larger box (panels D and E) were zoomed in for clarity.

Figure S2

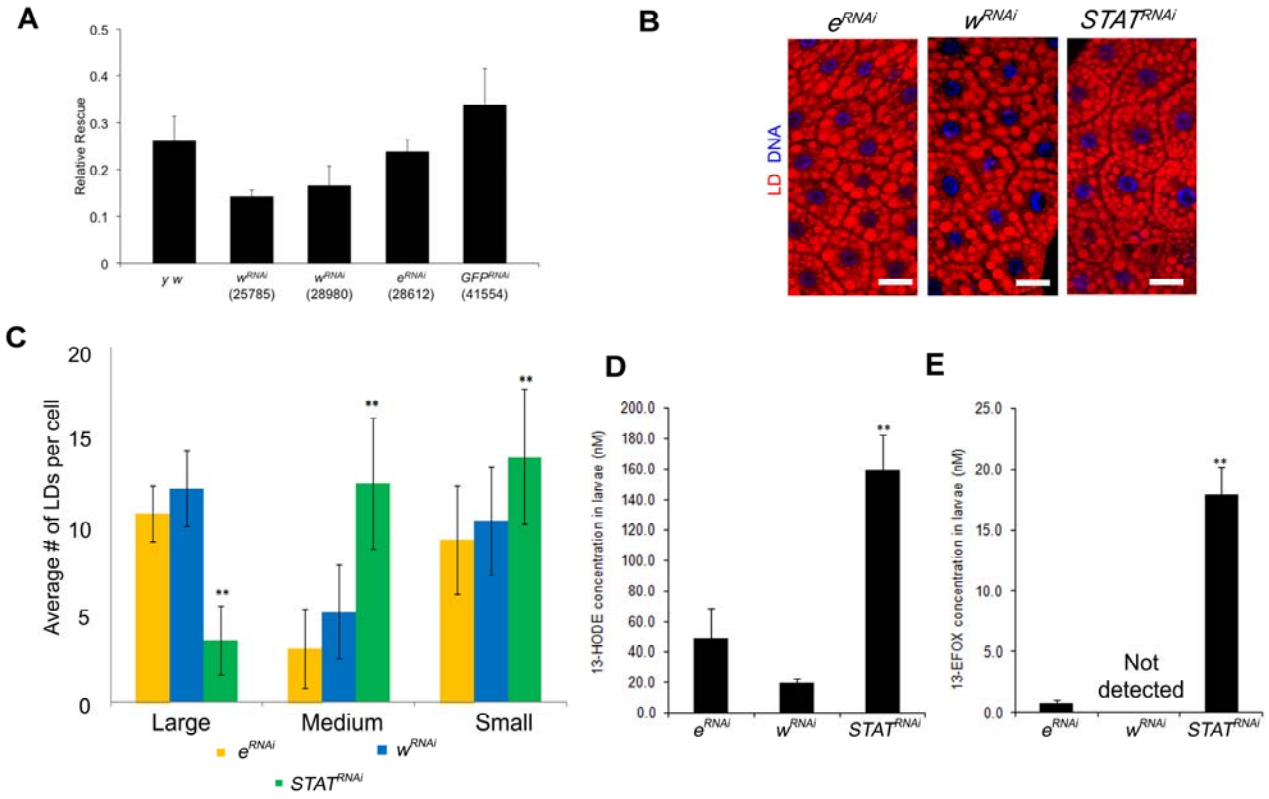

Fig. S2. Control experiments: Gene knockdown.
(A) Viability of control *hop*$^{Tum\text{-}l}$ *msn/Y; UAS-mCD8-GFP/+* males (born from a cross of *hop*$^{Tum\text{-}l}$ *msn-GAL4/FM7; UAS-mCD8-GFP* females with *y w/Y* males) compared to *hop*$^{Tum\text{-}l}$ *msn-GAL4/Y; UAS-mCD8-GFP/+* males expressing one copy of RNAi of *white*, *ebony*, or *GFP* raised at 27°C. The proportion of observed mutant males relative to *FM7/Y* balancer class is shown. Pairwise comparison of the proportion of surviving *hop*$^{Tum\text{-}l}$ males expressing RNAi with the *y w* outcross shows no significant difference ($p > 0.05$; *p*-values ranged from 0.10 to 0.71, student *t*-test; mean ± standard error). Three biological replicates with at least 100 males in each replicate are represented. Error bars are standard errors.
(B, C) Nile red-stained fat bodies (B) and average number of LD size categories per fat body cell (C) from progeny of homozygous *hop*$^{Tum\text{-}l}$ females crossed with *y w* males or males homozygous for UAS-*white*^{RNAi}, *ebony*^{RNAi}, or *STAT*^{RNAi} transgenes. Bars represent mean ± standard deviation computed across three biological replicates; $n > 100$ cells, 6 animals each; $^{**}p < 0.001$, student *t*-test.
(D, E) 13-HODE and 13-EFOX-L2 levels in larval extracts of animals with genotypes in panel B and C (mean ± standard deviation; $n > 200$ larvae per replicate; $^{**}p < 0.05$ across three biological replicates, one-way ANOVA).

Figure S3

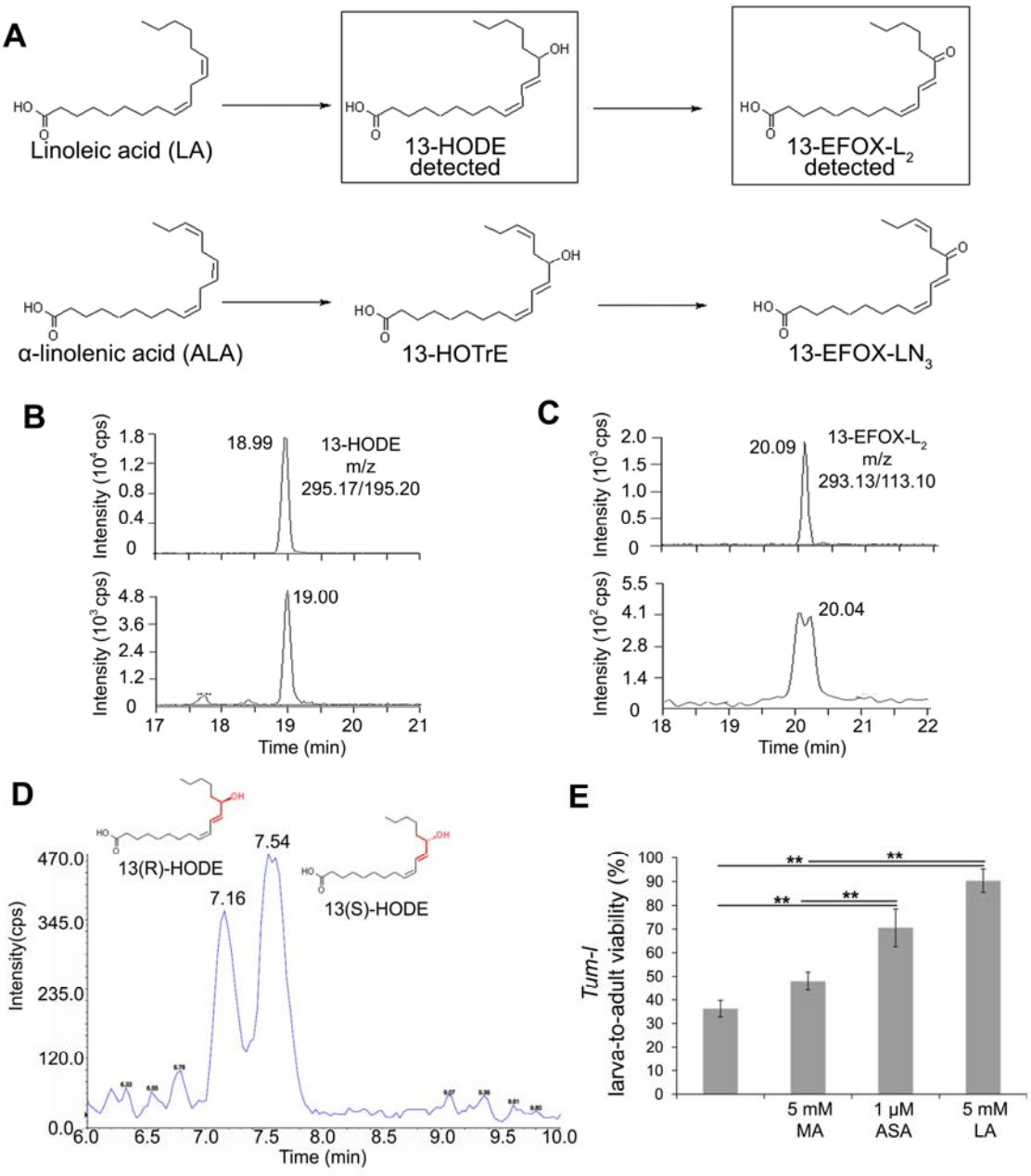

Fig. S3. Lipidomics analysis and larva-to-adult viability.
(A) Proposed biochemical mechanism based on the scheme (Groeger et al., 2010 ***Nat Chem Biol*** 6**, 433-41)** shows LA and ALA conversion to 13-HODE and 13-HOTrE,

respectively by COX-2 action. These are then further oxidized to 13-EFOX-L_2 and 13-EFOX-LN_3, respectively, via dehydrogenase enzymes.
(B) MRM scans monitoring for the m/z transitions 295.17/195.20 (MW of 13-HODE/loss of 99.97 m/z, see Fig. S4A) for standard 13-HODE (top panel) and a representative lipid sample (bottom panel).
(C) MRM scans monitoring for the m/z transitions 293.13/113.10 (MW of 13-EFOX-L_2 /loss of 180.03 m/z, see Fig. S4A) for standard 13-EFOX-L_2 (top panel), and a representative lipid sample (bottom panel).
(D) Chiral LC-MS analysis of larval extracts from 1 μM aspirin-treated *hop*$^{Tum\text{-}l}$ animals. Representative chiral chromatogram showing two-fold enantiomeric excess of 13(S)-HODE observed in larval extracts of wild type and mutant animals. This enantiomeric excess of 13(S)-HODE was also observed in aspirin-treated animals.
(E) Effect of myristic acid (MA), aspirin or linoleic acid (LA) treatment on viability of *hop*$^{Tum\text{-}l}$ *msn>mCD8-GFP* larvae compared to viability of untreated mutants (left bar). Effects of LA are slightly stronger than those of 1 μM aspirin, while MA's effects are not significant. The proportion of larvae that survived to adulthood was determined in three biological replicates; the number of larvae examined in each replicate ranged from 38 to 68 (mean ± standard deviation; student *t*-test). Statistically significant differences ($p < 0.05$; student *t*-test) are shown across three or four biological replicates.

Figure S4

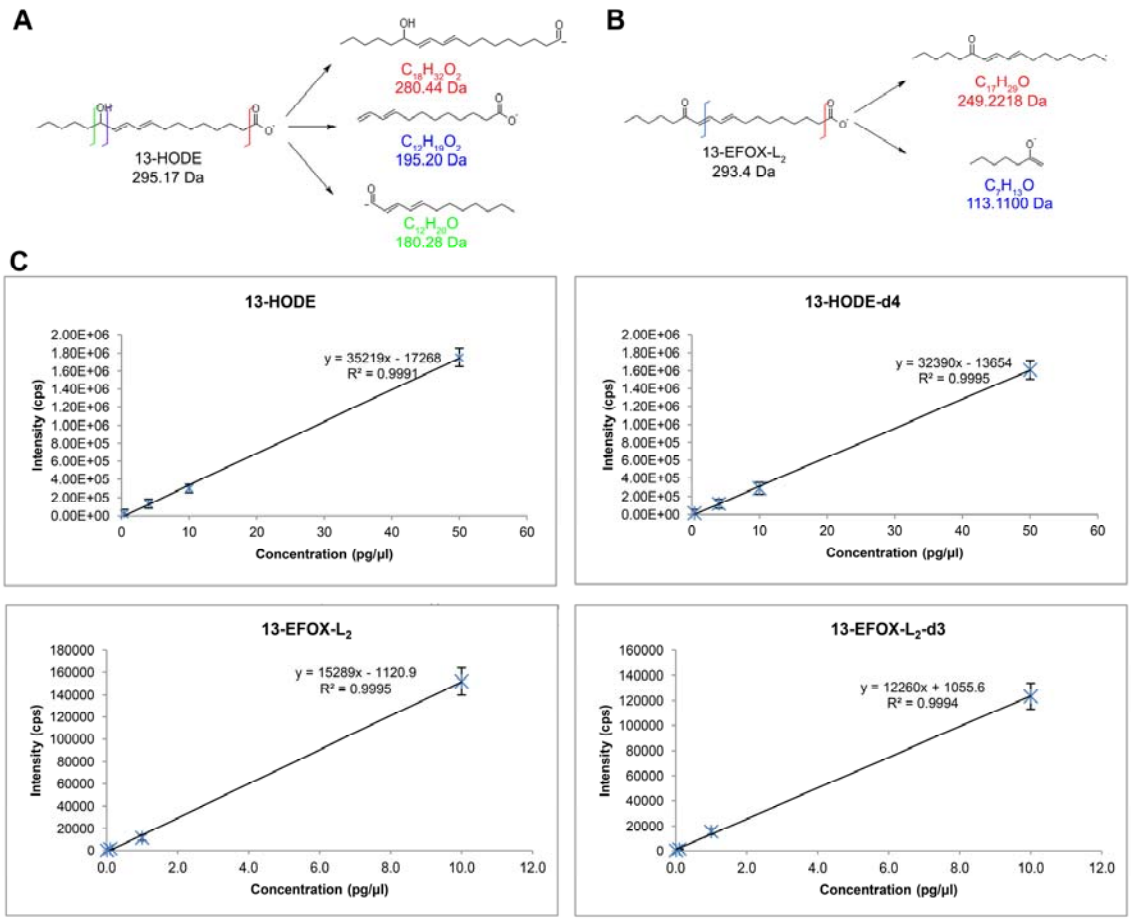

Fig. S4. Fragments selected for MS/MS analysis and calibration curves.
(A, B) Detection of 13-HODE (A) and 13-EFOX-L_2 (B) in MRM mode was based on the structures of the fragments shown. Such fragments were chosen experimentally after ascertaining that they represented the ones forming with the highest yield during the MS/MS analysis.
(C) Calibration curves for quantification of the bioactive lipids. The concentrations used to make the calibration curves for 13-HODE-d_4 and 13-HODE are 0.4, 4, 10, and 50 pg/µl whereas 0.01, 0.1, 1, and 10 pg/µl concentrations were used to prepare calibration curves for 13-EFOX-L_2-d_3 and 13-EFOX-L_2. The experimental samples were diluted so that analyte concentration was within the linear range (mean ± standard deviation, $n = 6$ samples per analyte per concentration).

Table S1. Mass spectrometry parameters for Multiple Reaction Monitoring.

Compound	Q1 Mass (Da)	Q2 Mass (Da)	DP (Volts)	CE (Volts)
13-HODE	295.170	280.400	-90	-26
	295.170	195.200	-90	-26
	295.170	180.300	-90	-28
13-EFOX-L_2	293.130	249.200	-90	-26
	293.130	113.100	-100	-28
13-HODE-d4	299.170	281.200	-95	-26
	299.170	230.800	-95	-16
	299.170	198.100	-95	-26
13-EFOX-L_2-d3	296.230	252.200	-90	-26
	296.230	114.100	-95	-29